Original research

# Precancerous nature of intestinal metaplasia with increased chance of conversion and accelerated DNA methylation

Chihiro Takeuchi,[1,2,3] Satoshi Yamashita,[1,4] Yu-Yu Liu,[1,2] Hideyuki Takeshima,[1,2] Akiko Sasaki,[1,5] Masahide Fukuda,[1,6] Taiki Hashimoto,[7] Tomoaki Naka,[7] Kenichi Ishizu,[8] Shigeki Sekine ,[7] Takaki Yoshikawa,[8] Akinobu Hamada,[9] Nobutake Yamamichi,[3,10] Mitsuhiro Fujishiro,[3] Toshikazu Ushijima [1,2]

► Additional supplemental material is published online only. To view, please visit the journal online (http://dx.doi.org/10.1136/gutjnl-2023-329492).

For numbered affiliations see end of article.

**Correspondence to**
Dr Toshikazu Ushijima, Hoshi University, Shinagawa-ku, Tokyo, Japan;
tushijima142@hoshi.ac.jp

Received 13 January 2023
Accepted 31 August 2023
Published Online First
26 September 2023



**To cite:** Takeuchi C, Yamashita S, Liu Y-Y, *et al*. *Gut* 2024;**73**:255–267.

## ABSTRACT

**Objective** The presence of intestinal metaplasia (IM) is a risk factor for gastric cancer. However, it is still controversial whether IM itself is precancerous or paracancerous. Here, we aimed to explore the precancerous nature of IM by analysing epigenetic alterations.

**Design** Genome-wide DNA methylation analysis was conducted by EPIC BeadArray using IM crypts isolated by Alcian blue staining. Chromatin immunoprecipitation sequencing for H3K27ac and single-cell assay for transposase-accessible chromatin by sequencing were conducted using IM mucosa. *NOS2* was induced using Tet-on gene expression system in normal cells.

**Results** IM crypts had a methylation profile unique from non-IM crypts, showing extensive DNA hypermethylation in promoter CpG islands, including those of tumour-suppressor genes. Also, the IM-specific methylation profile, namely epigenetic footprint, was present in a fraction of gastric cancers with a higher frequency than expected, and suggested to be associated with good overall survival. IM organoids had remarkably high *NOS2* expression, and *NOS2* induction in normal cells led to accelerated induction of aberrant DNA methylation, namely epigenetic instability, by increasing DNA methyltransferase activity. IM mucosa showed dynamic enhancer reprogramming, including the regions involved in higher *NOS2* expression. *NOS2* had open chromatin in IM cells but not in gastric cells, and IM cells had frequent closed chromatin of tumour-suppressor genes, indicating their methylation-silencing. *NOS2* expression in IM-derived organoids was upregulated by interleukin-17A, a cytokine secreted by extracellular bacterial infection.

**Conclusions** IM cells were considered to have a precancerous nature potentially with an increased chance of converting into cancer cells, and an accelerated DNA methylation induction due to abnormal *NOS2* expression.

### WHAT IS ALREADY KNOWN ON THIS TOPIC

⇒ The presence of intestinal metaplasia (IM) is a risk factor for gastric cancer.
⇒ Recent studies using bulk samples showed the presence of genetic and epigenetic alterations in tissues with IM.
⇒ It is still controversial whether IM itself is a precancerous or paracancerous lesion.

### WHAT THIS STUDY ADDS

⇒ With crypt isolation, IM cells had a unique DNA methylation profile, especially extensive hypermethylation in promoter CpG islands, including those of tumour-suppressor genes.
⇒ The IM-specific methylation profile, namely epigenetic footprint, was present in gastric cancer more frequently than expected, and was suggested to be associated with good overall survival.
⇒ IM cells suffer from accelerated induction of aberrant DNA methylation, namely epigenetic instability, likely due to increased *NOS2* expression and resultant increased DNA methyltransferase activity.
⇒ The *NOS2* expression was induced by enhancer reprogramming and chromatin opening, and was upregulated through interleukin-17A signalling.

### HOW THIS STUDY MIGHT AFFECT RESEARCH, PRACTICE OR POLICY

⇒ IM cells were considered to have a precancerous nature with an increased chance of converting into cancer cells and accelerated induction of aberrant DNA methylation.
⇒ The better survival of patients with IM cell-derived cancer after chemotherapy may lead to isolation of genes responsible for the better response.
⇒ Prevention of DNA methylation induction is expected to reduce the chance of gastric cancer development.

## INTRODUCTION

The presence of intestinal metaplasia (IM) is a risk factor for gastric cancer (GC), which confers a more than twofold increased cancer risk.[1] However, it is still controversial whether IM itself is precancerous or paracancerous. Based on the Correa hypothesis, GC develops in stages through chronic gastritis and IM, which considers IM as a precancerous lesion.[2] In addition, tissues with IM were reported

to have genetic and epigenetic alterations, using bulk samples,[3 4] suggesting the precancerous nature of IM. On the other hand, based on the gastric mucin phenotype, only 30% of GCs show an intestinal phenotype, despite developing from gastric tissue with IM,[5] suggesting the paracancerous nature of IM. In addition, IM had rare *TP53* mutations[3 6] whereas other types of mucosa with inflammation-associated carcinogenesis, such as UC and Barrett's oesophagus, had frequent *TP53* mutations,[7 8] which attenuates the precancerous nature of IM.

To address this long-standing question, we focused on DNA methylation. Chronic gastritis by *Helicobacter pylori* infection induces aberrant DNA methylation of a large number of genes in epithelial cells,[9–11] and the degree of aberrant methylation is correlated with cancer risk.[12–15] Although bulk mucosa samples with IM showed higher methylation levels than those without,[3 4] it is still unknown whether, at the cellular level, IM cells have a higher or unique methylation profile. If an IM-specific methylation profile, namely epigenetic footprint, exists, we can assess the precancerous nature of IM by analysing whether GCs have a higher chance of having such an IM-specific methylation profile than expected. In addition, higher frequencies of methylation-silencing of tumour-suppressor genes in IM cells than in gastric cells also support the precancerous nature of IM cells. More importantly, if induction of aberrant DNA methylation in IM cells is accelerated compared with that in gastric cells, this status can be termed as epigenetic instability, and will strongly support the precancerous nature of IM. It is well known that accelerated induction of mutations due to inactivation of mismatch repair genes (microsatellite instability (MSI)) confers a precancerous nature to cells with MSI.[16 17]

In this study, we aimed to explore whether IM cells themselves are precancerous or paracancerous. First, we will investigate whether an IM-specific methylation profile is present using purely isolated IM crypts, and whether the specific profile is carried into GCs more frequently than expected. Second, we will analyse accelerated DNA methylation induction in IM cells, along with its underlying mechanisms.

## MATERIALS AND METHODS

### Samples obtained from surgical specimens, crypt isolation and organoid establishment

Gastric mucosa was freshly obtained with written informed consent from 11 patients with GC who underwent gastrectomy, 1 patient with a GI stromal tumour and 1 sample of small intestine was obtained from a neuroendocrine tumour patient at the National Cancer Center (online supplemental figure S1 and online supplemental table S1). The gastric mucosa was used for chromatin immunoprecipitation sequencing (ChIP-seq) and single-cell assay for transposase-accessible chromatin by sequencing (ATAC-seq) (online supplemental methods).

Gastric and intestinal crypts were further prepared from the mucosa for DNA methylation analysis. Gastric crypts were stained with an Alcian Blue Stain Kit (Abcam, Cambridge, UK) to distinguish IM crypts from non-IM crypts, and the crypts positive for staining of goblet cells were considered as IM crypts. Six gastric crypt samples of IM (IM_1–6) and eight samples of non-IM (non-IM_1–4 and 8–11) were prepared from 10 patients with GC, and 1 normal gastric crypt (Normal_12) and one small intestinal crypt (SI_13) samples were also prepared (online supplemental table S1).

Organoids were established from four gastric mucosa with IM (IM_2–4 and 6) and four without (non-IM_2 and 8–10) (online supplemental methods).

### Mucosa biopsy samples

Eight biopsy samples of gastric mucosa were obtained from healthy volunteers without *H. pylori* infection, and 19 samples with current *H. pylori* infection. These samples were used for gene expression analysis.

### Data acquisition from public data repository

Genome-wide DNA methylation profiles of small intestinal crypts (accession #GSE141254),[18] blood cells (accession #GSE35069),[19] biopsy samples (accession #GSE103186),[20] human cell lines (accession #GSE68379),[21] primary GCs and the corresponding adjacent mucosa (accession #GSE127857 and #GSE164988)[22 23] were obtained from the Gene Expression Omnibus (GEO). Single-cell RNA-sequencing (RNA-seq) data of IM mucosa samples (accession #GSE134520)[24] was obtained from the GEO.

### Genome-wide DNA methylation analysis

Genome-wide DNA methylation analysis was performed using an Infinium MethylationEPIC array (Illumina, California, USA).[25] Obtained β-values, ranging from 0 (unmethylated) to 1 (fully methylated), were normalised as previously described.[26] For cancer samples, the methylation levels were normalised by the cancer cell fraction obtained by methylation levels of marker genes.[27 28]

### Patient and public involvement

Patients and/or the public were not involved in the design, or conduct, or reporting, or dissemination plans of this research.

See online supplemental methods for more details.

## RESULTS

### Extensive methylation changes in IM crypts, involving tumour-suppressor genes

Genome-wide DNA methylation analysis was conducted using pure gastric crypts with and without IM (IM and non-IM crypt samples) (figure 1A).[29] The IM and non-IM crypt samples from the same patient showed distinct DNA methylation profiles while the IM (or non-IM) crypt samples from different patients showed similar methylation profiles (figure 1B and online supplemental figure S2A), showing the presence of a distinct but consistent methylation profile in IM. Cluster analysis was conducted using the crypt samples of IM (n=6), non-IM (n=8), normal stomach (n=1) and small intestine (n=6). Using the 20 000 CpG sites in all genomic regions and CpG shore with the highest SD, which is reported to be associated with tissue specificity,[30] the IM crypt samples were separated from the non-IM crypt samples and were clustered with the small intestinal crypt samples (figure 1C left and online supplemental figure S2B left). Also, using the 2000 CpG sites in promoter and intergenic CpG islands (CGIs), the IM crypt samples were clearly separated from the non-IM and small intestinal crypt samples, showing the presence of hypermethylation of CGIs in IM crypts (figure 1C right and online supplemental figure S2B right).

To analyse methylation-silencing of individual genes, we compared the average β-values of CpG sites within promoter CGIs among the samples. The IM crypt samples showed extensive hypermethylation compared with the non-IM samples and with small intestinal crypt samples (figure 1d, online supplemental figure S2C). Pathway enrichment analysis (DAVID) using the genes with differentially methylated promoter CGIs ($\Delta\beta \geq 0.1$ and $p<0.05$) between the IM and non-IM crypt samples (online supplemental table S2) identified 16 terms (cut-off value=0.01), including

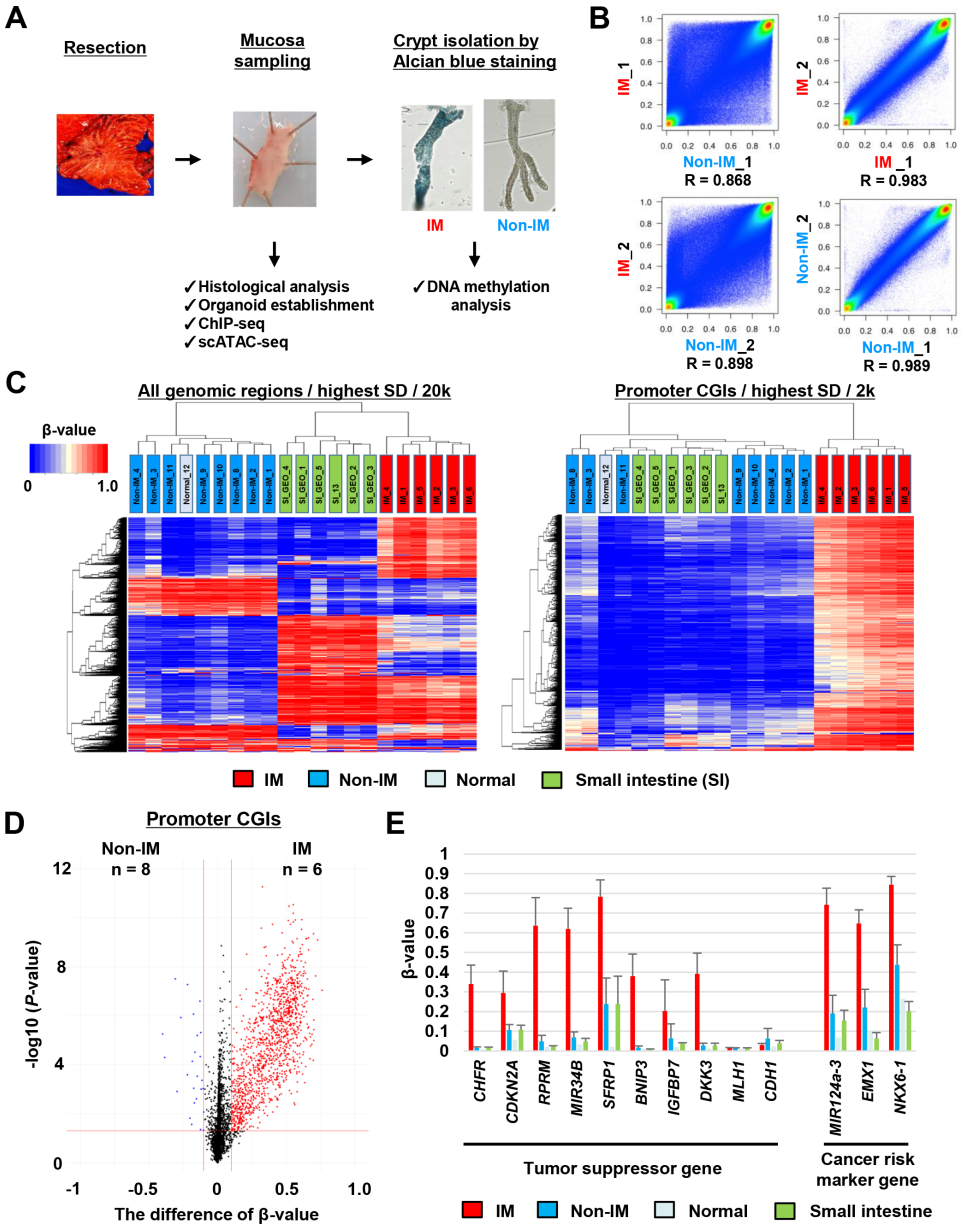


**Figure 1** Extensive DNA methylation changes in intestinal metaplasia (IM) crypts. (A) Scheme of mucosa collection from a resected specimen and isolation of crypts with and without IM. (B) Scatter plot analysis using methylation levels of total CpG sites. The IM and non-IM crypt samples from the same patient showed distinct DNA methylation profiles while the IM (or non-IM) crypt samples from different patients showed similar methylation profiles. Patient numbers are shown after 'IM_' or 'non-IM_'. (C) Unsupervised hierarchical cluster analysis using the methylation levels of the crypt samples of IM (n=6), non-IM (n=8), normal stomach (n=1) and small intestine (n=6). Left panel: using the 20 000 CpG sites in all genomic regions with the highest SD (HSD), the IM crypt samples were separated from the non-IM crypt samples, and were clustered with the small intestinal crypt samples. Right panel: using the 2000 CpG sites located in promoter CpG islands (CGIs), the IM crypt samples were clearly separated from the non-IM and small intestinal crypt samples. (D) Volcano plot analysis using DNA methylation levels of genomic blocks in promoter CGIs. The IM crypt samples showed extensive DNA hypermethylation compared with the non-IM crypt samples. (E) DNA methylation levels of tumour-suppressor and cancer risk marker genes. Regarding the tumour-suppressor genes, the IM crypt samples showed the highest methylation levels. Regarding the cancer risk marker genes, the methylation levels increased in the order of normal gastric crypts, non-IM crypts and IM crypts. Data represent mean±SE.

the Wnt signalling pathway (online supplemental table S3). We explored motives of transacting factors enriched in the differentially methylated promoter CGIs, but no motif was enriched (online supplemental table S4).

We also analysed methylation levels of individual genes, especially tumour-suppressor genes, which have been extensively studied in the major pathways altered in GC with at least three publications addressing their involvement.[31] The IM crypt samples showed the highest methylation levels, while the non-IM gastric crypt samples showed methylation levels between the IM and normal crypt samples. Regarding the cancer risk marker genes, whose methylation levels were reported to be highly correlated with cancer risk[12 13] and genome-wide methylation alterations[31] (figure 1E), the methylation levels increased in the order of normal crypts, non-IM crypts and IM crypts. On the other hand, promoter CGIs of *CDX2*, *ASCL2*, *WNK2*, *EGFL7* and *EDN3* were found to be unmethylated in IM and small intestinal crypt samples, but methylated in non-IM crypt samples (online supplemental table S5).

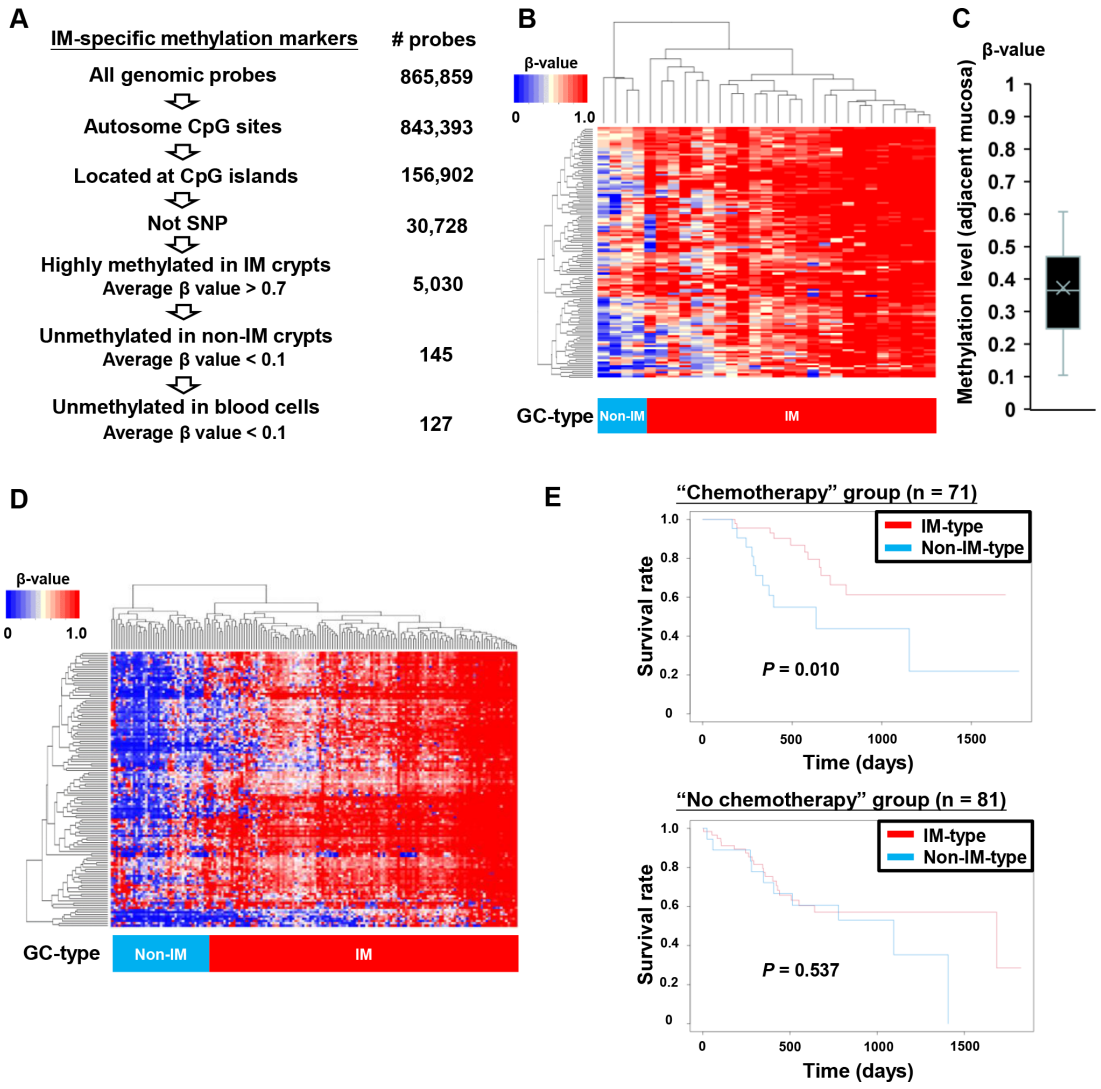


**Figure 2** Extraction of an intestinal metaplasia (IM)-specific methylation profile, and its presence in gastric cancer (GC) with high probabilities. (A) Screening scheme of IM-specific methylation markers. (B) Unsupervised cluster analysis of GCs using the IM-specific methylation markers. The GC samples were clearly separated into two groups, IM-type (n = 25) and non-IM-type (n = 4) GCs. The proportion of IM-type GCs was 25/29 (86%). (C) Distribution of the average methylation levels of IM-specific markers in the adjacent mucosa, which corresponded with the proportion of IM cells. The mean methylation level was 37±14% (mean±SE). The incidence of IM-type GCs (86%) was higher than expected based on the mean IM-cell proportion (37%), indicating that IM cells have a higher chance of developing into cancer cells than non-IM cells. (D) Unsupervised cluster analysis using the IM-specific methylation markers. The GC samples from The Cancer Genome Atlas database were clearly separated into the two groups, IM-type and non-IM-type GCs. (E) Kaplan-Meier analysis of patients with GC with and without chemotherapy. Among the patients with chemotherapy (n=71), the patients with IM-type GC appeared to have better overall survival than those with non-IM-type GC (p=0.010). On the other hand, among the patients without (n=81), there was no difference (p=0.537).

### Frequent presence of the IM-specific methylation profile in gastric cancer

Next, we searched for IM-specific methylation markers, namely CpG sites within CGIs methylated in the IM crypt samples (average β>0.7) and unmethylated in the non-IM crypt samples and the blood cell samples[19] (average β<0.1), and identified 127 CpG sites in 118 CGIs (figure 2A and online supplemental table S6). Using the GEO database (accession #GSE103186),[20] these markers had high methylation levels in IM biopsy samples but not in normal biopsy samples (online supplemental figure S3A). Using these markers, GC samples from our previous studies[32 33] and the GEO database[22 23] (accession #GSE127857 and #GSE164988) were clearly separated into two groups, IM-type (n=25) and non-IM-type (n=4) groups (figure 2B), indicating that the IM-specific methylation profile, namely epigenetic footprint, was carried into a fraction of GCs.

Cancer cells are expected to have the methylation profile of their precursor clone. Therefore, if a patient's cancer is derived from a precursor clone with IM, the cancer is expected to exhibit an IM-specific methylation profile. To investigate whether cancer cells were derived from IM cells more frequently than from non-IM cells, we compared the incidence of IM-type GCs in a panel of patients and the proportion of IM cells in their total background gastric mucosa (online supplemental figure S3B). The proportion of IM cells in the background mucosa can be calculated by the average methylation levels of IM-specific markers. Resultantly, the incidence of IM-type GCs (25/29=86%) (figure 2B) was higher than expected based on

the mean IM-cell proportion (37%) (figure 2C), indicating that IM cells have a higher chance of developing into cancer cells than non-IM cells. Although there is a possibility of methylation profile change in cancer cells, these findings supported the precancerous nature of IM cells.

The presence of the IM-specific methylation was validated using methylation data normalised for cancer cell fraction of primary GC samples from the Genomic Data Commons Data Portal (https://portal.gdc.cancer.gov/) and IM-specific methylation markers. The samples were clearly separated into two groups, IM-type and non-IM-type groups (figure 2D, online supplemental tables S7 and S8). Taking advantage of the availability of their prognostic information, it was shown that the patients with IM-type GC tended to have better overall survival (OS) than those with non-IM-type GC (p=0.084) (online supplemental figure S3C). Notably, among the patients with chemotherapy (n=71), the patients with IM-type GC appeared to have better OS than those with non-IM-type GCs (p=0.010). On the other hand, among the patients without chemotherapy (n=81), there was no difference in OS (p=0.537) (figure 2E). These data suggested that an IM-specific methylation profile might contribute to drug sensitivity.

To address this hypothesis, we analysed 29 GC cell lines using the 127 IM-specifically methylated CpG sites. The cell lines were separated into 26 IM-type and 3 non-IM-type ones (online supplemental figure S4A). We picked up two IM-type cell lines with high methylation and two non-IM-type cell lines randomly, and analysed their sensitivity to 5-fluorouracil (5-FU), a commonly used chemotherapeutic agent against GC.[34] As expected, the two IM-type cell lines (AGS and 44As3) showed higher sensitivity than the two non-IM-type, cell lines (GCIY and HSC60) (online supplemental figure S4B). These data suggested that an IM-specific methylation profile in GC is associated with good prognosis, possibly conferring sensitivity to chemotherapeutic agents, such as 5-FU.

### Abnormal gene expression involved in aberrant DNA methylation in IM

To explore the inducer of aberrant DNA methylation in IM, we analysed expression of inflammation-related genes known to be involved in DNA methylation induction[10 35 36] using our mucosal biopsy samples. Tumour necrosis factor (*TNF*) and interleukin (*IL)1B* were highly expressed in gastric mucosa with current *H. pylori* infection. On the other hand, *NOS2* was highly expressed in only a fraction of the samples, and the *NOS2* expression was highly associated with those of IM-specific genes (*CDX1*, *CDX2* and *MUC2*) (figure 3A), suggesting that IM cells might express endogenous *NOS2*. This was supported by the analysis of single-cell RNA-seq data of IM mucosa samples with current *H. pylori* infection in the GEO database (accession #GSE134520)[24] (online supplemental figure S5A). *NOS2*-positive cells were detected only in three *H. pylori*-positive samples (online supplemental figure S5B), and overlapped with *CDX2*-positive cells (online supplemental table S9). Also, immunohistochemistry of IM mucosa samples showed that NOS2 was highly expressed in IM crypts, but not in non-IM crypts (figure 3B).

To confirm the *NOS2* expression in IM cells, we established organoids from four gastric mucosa with IM and four without. Morphologically, the IM-derived organoids exhibited a smooth round shape-like gastric organoids as previously reported.[37] The IM-derived organoids contained a large fraction of organoids that secreted intestinal-type mucin in apical spaces, as confirmed by Alcian blue staining (figure 3C). The IM-derived organoids showed higher *NOS2* expression than the non-IM-derived organoids did, and *NOS2* expression was highly correlated with *CDX2* expression (figure 3D).

### *NOS2* induction in normal cells accelerates aberrant DNA methylation induction

To examine whether endogenous *NOS2* expression accelerates aberrant DNA methylation induction, *NOS2* was induced using a Tet-on expression system in normal cells, 293FT and HGEC6B cells. Doxycycline (DOX) treatment at 10 ng/mL in 293FT and 1 ng/mL in HGEC6B induced physiological levels of *NOS2* expression (figure 4A) comparable to those in biopsy samples of gastric mucosa with IM (figure 3A), and the DOX-treated cells showed increased DNA methyltransferase (DNMT) activities compared with untreated cells and their parental cells (figure 4B).

After 10-week and 20-week cultures, we analysed the impact of *NOS2* induction on DNA methylation profile.[29] DOX-treatment, which itself has no inherent effect (online supplemental figure S6A), was shown to induce aberrant DNA methylation ($\Delta\beta \geq 0.2$) in a large number of CpG sites (figure 4C and online supplemental figure S6b), even after switching DOX-off (online supplemental figure S6C). The methylated CpG sites were mainly located in gene body regions without CGIs (figure 4D). Although CGIs are known to be resistant to methylation induction,[38] the number of hypermethylated CpG sites in CGIs became large at 20 weeks, especially in HGEC6B cells (figure 4E). On the other hand, NOC18 treatment, which mimics nitric oxide (NO exposure from leucocytes, induced slight DNA methylation (online supplemental figure S6D), indicating that IM cells suffer from extensive DNA methylation induction, namely epigenetic instability, by endogenous *NOS2* expression.

### Reprogramming of promoters and enhancers involved in abnormal *NOS2* expression in IM

To investigate the mechanisms involved in abnormal *NOS2* expression, we performed ChIP-seq of H3K27ac using a normal gastric mucosa sample (n=1) and IM mucosa samples (n=2) (figure 1A).[39] In the promoter and downstream regions of *CDX2*, which are critical for the IM phenotypes,[40] the IM mucosa samples showed large peaks, but the normal gastric mucosa sample showed almost no peaks (figure 5A). In the *NOS2* enhancer and promoter regions,[41 42] the IM mucosa samples showed increased H3K27ac peaks (figure 5B) compared with the normal gastric mucosa sample. The enhancer regions with the H3K27ac peaks were reported to be bound by RELA (online supplemental figure S7A), suggesting that IM cells underwent enhancer reprograming in *NOS2* upstream regions to respond to nuclear factor kappa B (NF-κB) signalling.[42]

We also identified 44 550 peaks gained in IM (IM-Gained), 18 218 peaks lost in IM (IM-Lost) and 24 503 common peaks (figure 5C), indicating that IM cells underwent dynamic reprogramming of promoters and enhancers. To interpret the regions enriched in IM-Gained and IM-Lost groups, we conducted functional annotation analysis using Genomic Regions Enrichment of Annotations Tools. The regions of the IM-Gained group included the genes for the biosynthetic process of NO while the regions of the IM-Lost group included the genes for the regulations of messenger RNA catabolic pathways and sodium ion transport (figure 5D).

When super-enhancers were analysed, the IM mucosa gained multiple super-enhancers, including one for *CDX2* (online supplemental figure S7B) and those for genes related to wound

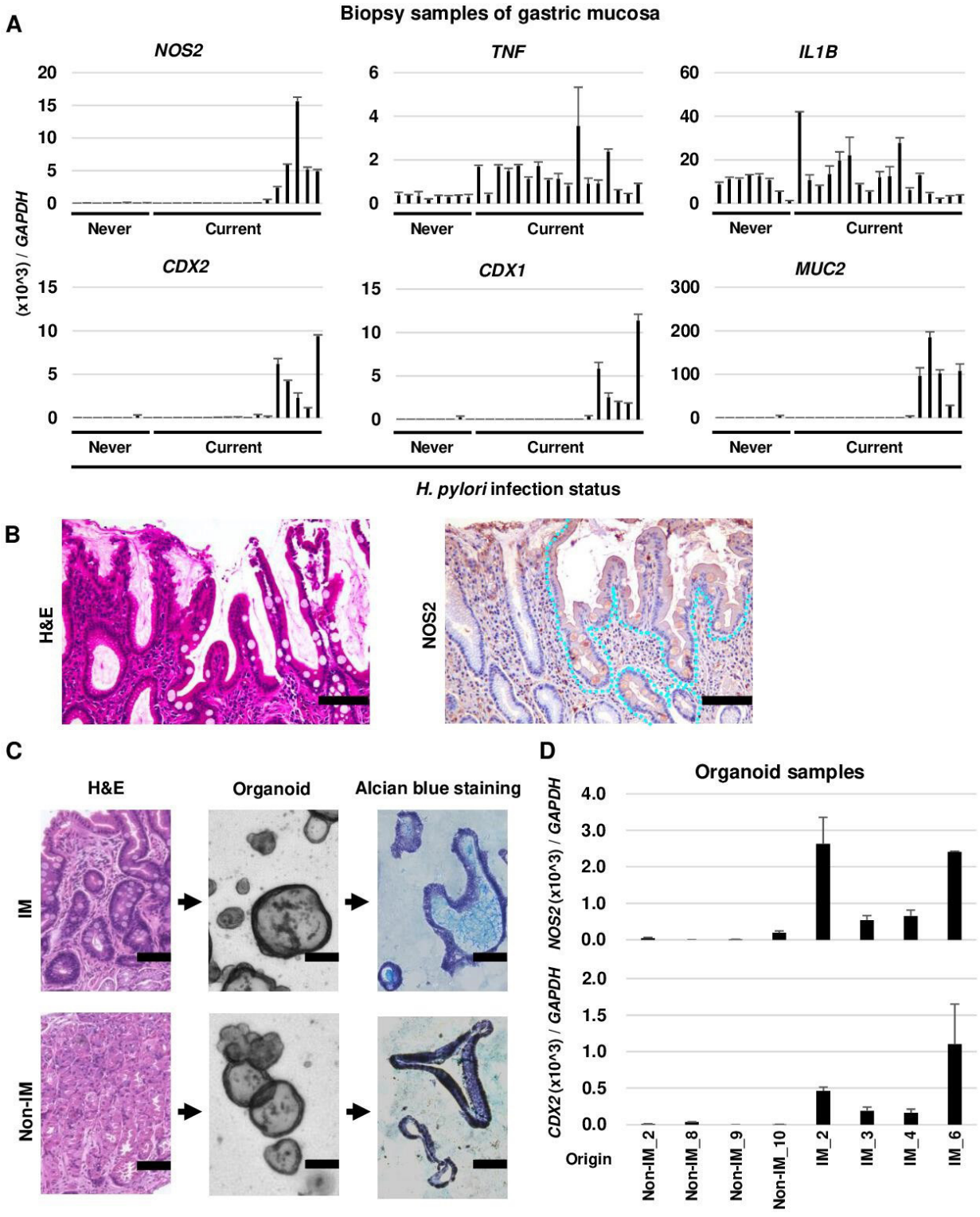


**Figure 3** Abnormal *NOS2* expression in intestinal metaplasia (IM). (A) Expression levels of inflammation-related genes (*NOS2*, tumour necrosis factor (*TNF*) and interleukin (*IL)-1B*) and IM-specific genes (*CDX2*, *CDX1* and *MUC2*) in mucosal biopsy samples according to *Helicobacter pylori* infection status (never-infected or currently infected). *NOS2* was highly expressed in a fraction of the samples with current *H. pylori* infection, and the *NOS2* expression was highly associated with those of IM-related genes. Data represent mean±SE. (B) Immunostaining of NOS2. NOS2 was highly expressed in IM, but not in non-IM crypts. Blue dotted lines encircle IM crypts. Scale bar: 100 µm. (C) Organoid establishment and Alcian blue staining. The IM-derived organoids contained a large fraction of organoids that secreted intestinal-type mucin in apical spaces, as confirmed by Alcian blue staining. (D) Expression levels of *NOS2* and *CDX2* in organoids. The IM-derived organoids showed higher *NOS2* expression than the non-IM-derived organoids did, and *NOS2* expression was highly correlated with *CDX2* expression. Data represent mean±SE.

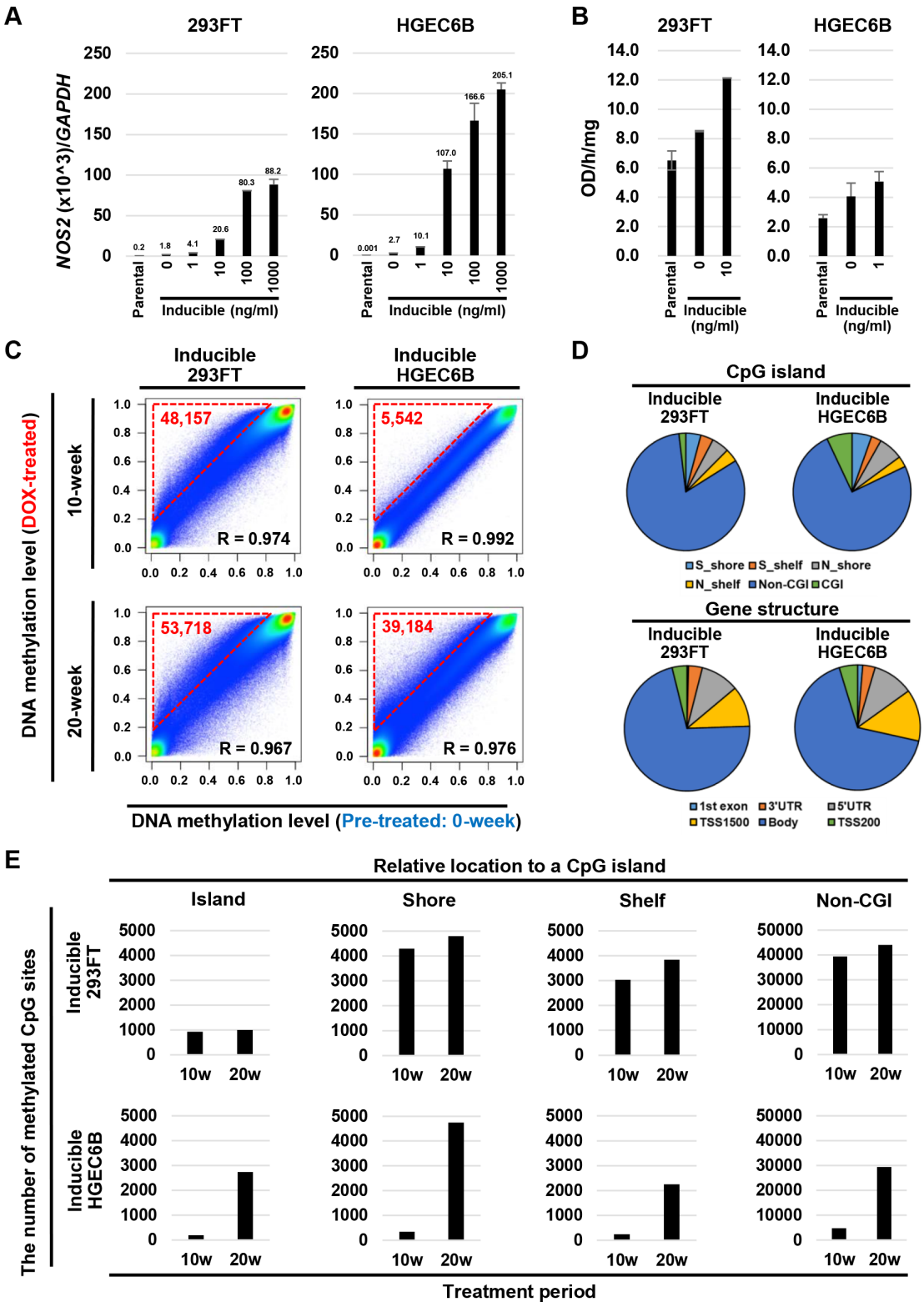


**Figure 4** DNA methylation induction by *NOS2* expression in normal cells. (A) Expression levels of *NOS2* according to the concentrations of doxycycline (DOX) in inducible cells (293FT and HGEC6B). Data represent mean±SE. (B) Increased DNA metyltransferase (DNMT) activity by *NOS2* induction in inducible cells (293FT and HGEC6B). DOX-treated cells showed increased DNMT activity compared with untreated cells and their parental cells. (C) DNA methylation analysis of DOX-treated (0 week and 20 weeks) and pretreated (0 week) inducible cells (293FT and HGEC6B). *NOS2* induction was shown to induce aberrant DNA methylation ($\Delta\beta \geq 0.2$) in a large number of CpG sites. The CpG sites with a $\beta \geq 0.2$ are in triangles with red broken lines, and their numbers are noted. (D) Characteristics of hypermethylated genomic regions in 293FT and HGEC6B cells. The methylated CpG sites were mainly located in gene body regions without CpG islands. (E) The number of hypermethylated CpG sites according to the relative location to a CpG island in 293FT and HGEC6B cells. The number of hypermethylated CpG sites in CpG islands became large at 20 weeks, especially in HGEC6B cells.

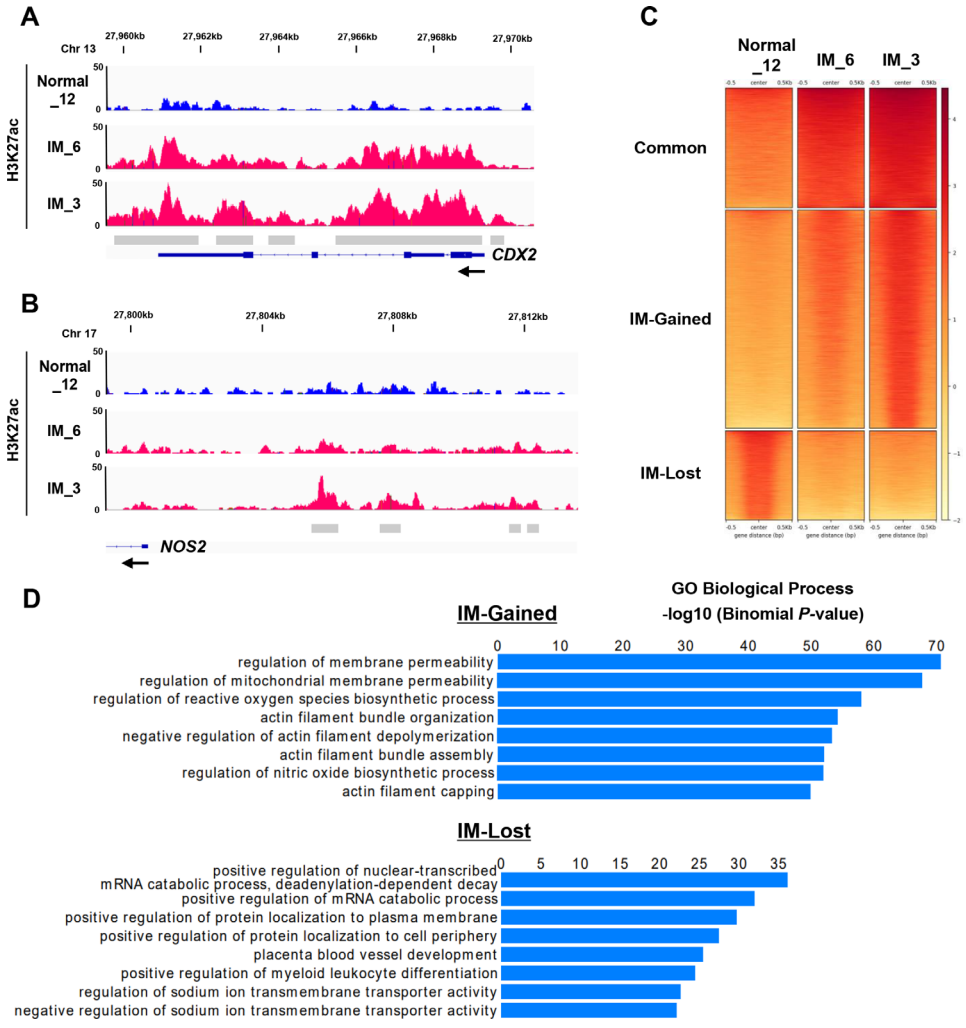


**Figure 5** Reprogramming of promoters and enhancers in intestinal metaplasia (IM) mucosa. (A, B) Genome browser views of chromatin immunoprecipitation sequencing (ChIP-seq) for H3K27ac using a normal gastric mucosa sample (n=1) and IM mucosa samples (n=2). In the *CDX2* promoter and downstream regions (A), the IM mucosa samples showed large peaks, but the normal gastric mucosa sample showed almost no peaks. Grey boxes represent genomic regions with detected peaks. In the *NOS2* enhancer and promoter regions (B), the IM mucosa samples showed increased H3K27ac peaks compared with the normal gastric mucosa sample. (C) K-means clustering (K=3) analysis of H3K27ac in the normal and two IM mucosa samples. Genomic regions that gained (IM-Gained) and lost (IM-Lost) H3K27ac, along with unchanged regions (common) were identified. (D) Gene ontology analysis by Genomic Regions Enrichment of Annotations Tools for the IM-Gained and IM-Lost genomic regions. A gene most proximal to a region with H3K27ac change was considered to be affected by the change. The eight enriched Gene Ontology (GO) annotations are shown. Statistics: one-sided binomial test.

healing and immune system development (online supplemental figure S7C).

### Changes of nucleosome positioning involved in abnormal *NOS2* expression and methylation-silencing in IM

Next, we performed single-cell ATAC-seq using a normal gastric mucosa sample and an IM mucosa sample (figure 1A).[43] A total of 9819 cells with adequate sequencing depths (>2000 reading fragments) and high transcription start site (TSS) enrichment score (>6) were obtained. The cells were grouped into 12 clusters by the similarities of chromatin opening (figure 6A) and the clusters were constructed by Uniform Manifold Approximation and Projection (UMAP) plot and the individual clusters were annotated by the pre-existing cell type-specific marker genes[44] (figure 6B and online supplemental table S10). In the promoter region of *CDX2*, IM-pit and IM-endocrine cells had open chromatin (figure 6C). IM-pit cells were grouped with gastric pit cells, gastric mucous neck cells and gastric chief cells while IM-endocrine cells, gastric endocrine cells and gastric parietal cells were isolated individually (figure 6A).

The enhancer region of *NOS2*, marked with H3K27ac binding peaks (figure 5B), had open chromatin in many cell types (figure 6D). In contrast, the *NOS2* promoter region had open chromatin specifically in IM-pit cells, but closed chromatin in all immune cells (figure 6D). This showed that *NOS2* was mainly expressed in IM-pit cells in the human stomach. Furthermore, promoter regions of tumour-suppressor genes, such as *RPRM*, had frequent closed chromatin in IM-pit cells compared with those in all types of gastric cells (Figure 6E and online supplemental figure S8), which supported the presence of aberrant DNA methylation of tumour-suppressor genes in IM crypts (figure 1E).

### IL-17A upregulates *NOS2* expression in IM

As *NOS2* expression is induced in macrophage or colonic epithelial cells by inflammatory cytokines,[41 42 45] such as TNF, IL-1β and IL-17A, we investigated which cytokine upregulated *NOS2*

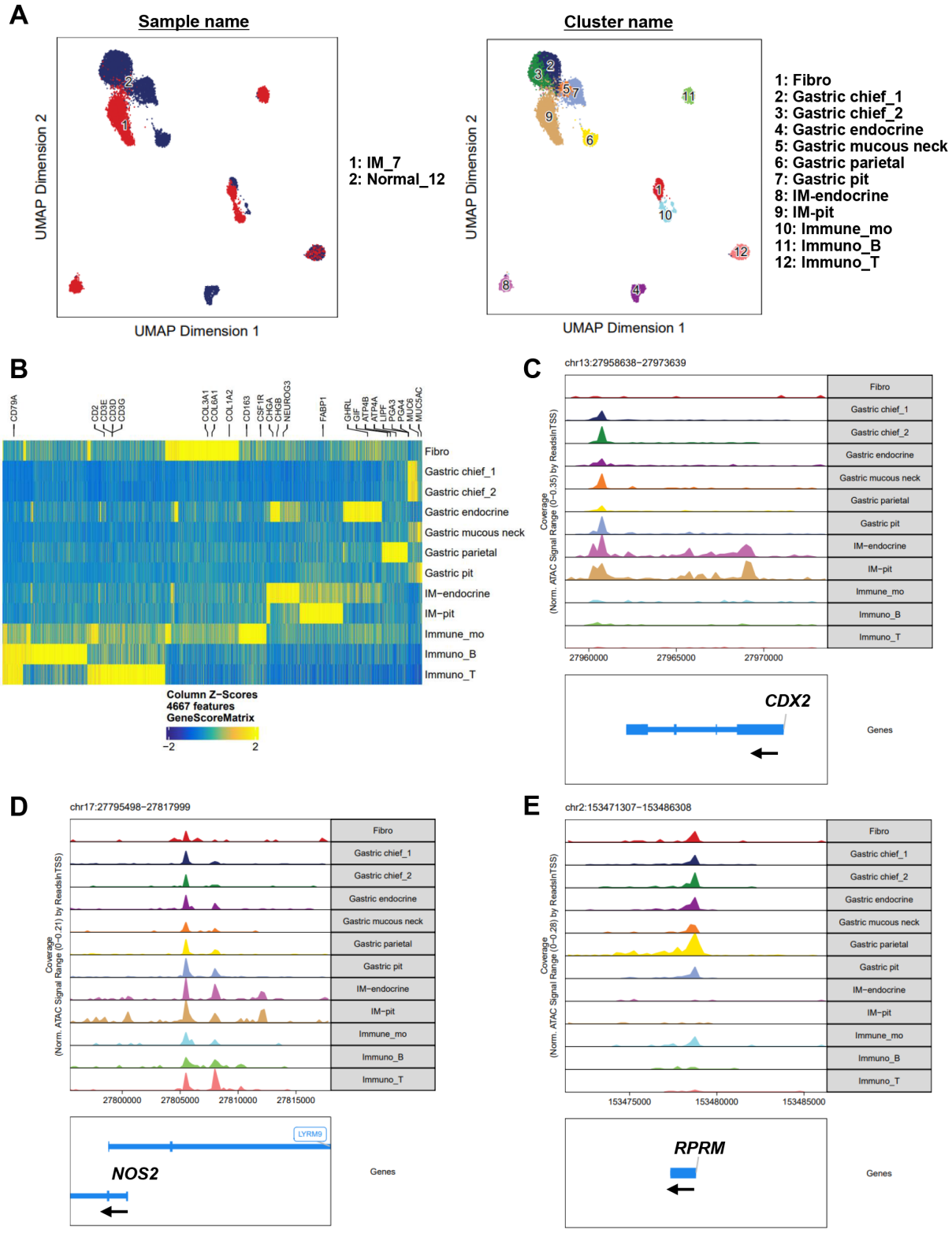


**Figure 6** Changes of chromatin statuses in intestinal metaplasia (IM) cells shown by single-cell assay for transposase-accessible chromatin by sequencing. (A) The UMAP plot of 9819 high-quality cells from a normal gastric mucosa sample (1: Normal_12) and an IM mucosa sample (2: IM_7). The cells are coloured based on the sample origins (left) and on the similarities of chromatin openings (right). (B) Heatmap to identify cell types based on chromatin openings assessed by gene scores. All the clusters were annotated by lineage-specific marker genes. 1, fibroblasts (Fibro); 2, chief cell group 1 (Gastric chief_1); 3, chief cell group 2 (Gastric chief_2); 4, gastric endocrine cells (Gastric endocrine); 5, mucous neck cells (Gastric mucous neck); 6, parietal cells (Gastric parietal); 7, gastric pit cells (Gastric pit); 8, IM-associated endocrine cells (IM-endocrine); 9, IM-associated pit cells (IM-pit); 10, monocytes (Immune-mo); 11, B cells (Immuno-B) and 12, T cells (Immuno-T). (C–E) Chromatin opening statuses in the upstream regions of the *CDX2* (C), *NOS2* (D) and *RPRM* (E) genes. IM-pit and IM-endocrine cells had open chromatin in the promoter region of *CDX2* (E). The *NOS2* promoter region had open chromatin specifically in IM-pit cells (D), but closed chromatin in all immune cells. The promoter regions of *RPRM* had closed chromatin in IM-pit cells compared with those in all types of gastric cells (E).

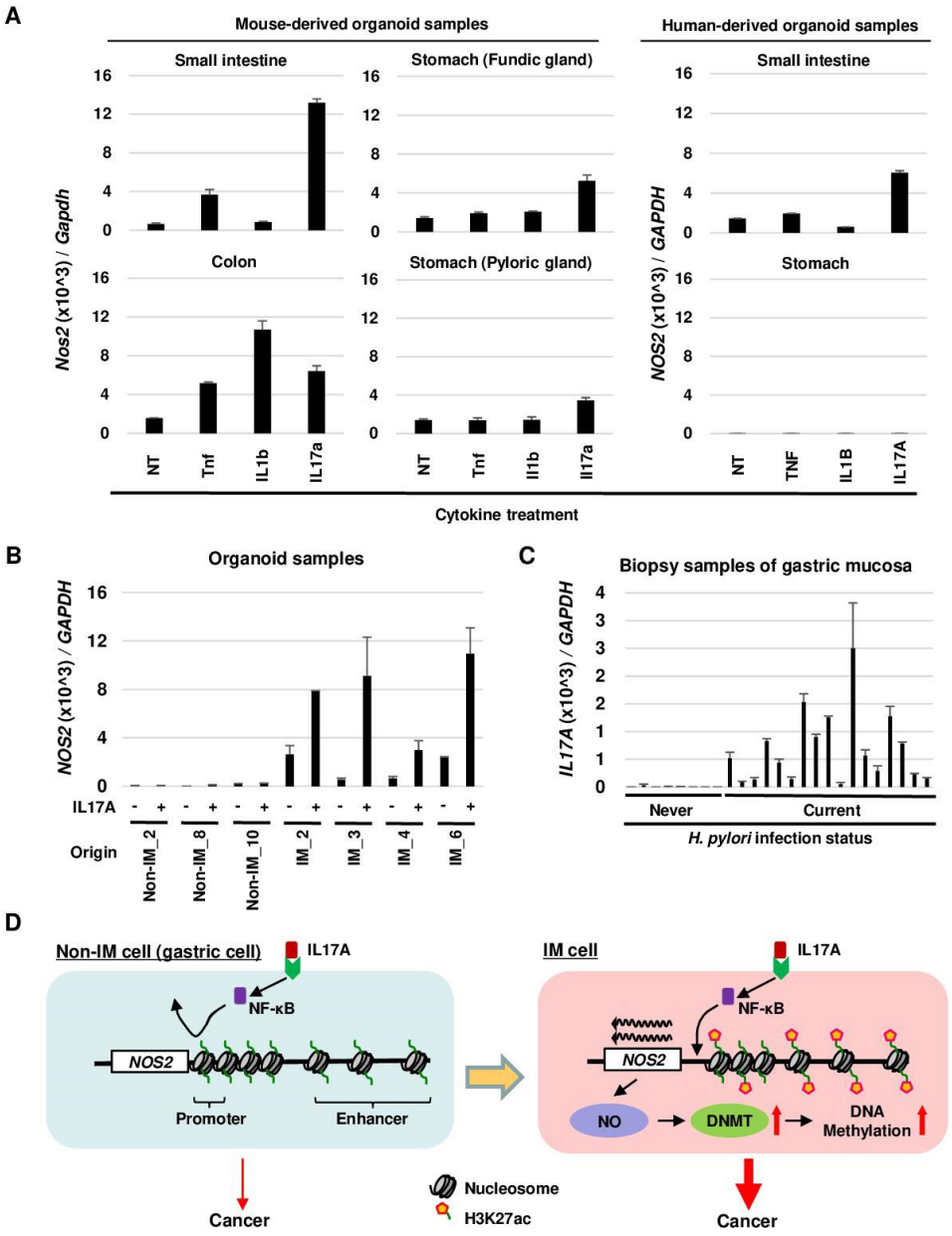


**Figure 7** *NOS2* induction by interleukin (IL)-17A in intestinal metaplasia (IM). (A) Expression levels of *Nos2* (or *NOS2*) after treatment with tumour necrosis factor (TNF), IL-1β or IL-17A in the intestine-derived and stomach-derived organoids. Left panel: among the mouse organoids derived from the small intestine, colon, fundic glands and pyloric glands, IL-17A upregulated *NOS2* expression very potently in those from small intestine. Right panel: in human-derived organoids, IL-17A upregulated *NOS2* expression in the small intestine-derived one, but not in the stomach-derived one. Data represent mean±SE. NT, not treated. (B) Expression levels of *NOS2* after IL-17A treatment in IM-derived or non-IM-derived organoids. IM-derived organoids showed *NOS2* induction by the treatment, while non-IM-derived organoids did not. Data represent mean±SE. (C) Expression levels of *IL17A* in mucosa samples according to *Helicobacter pylori* infection status (never-infected or currently infected). The mucosal biopsy samples with current *H. pylori* infection showed high *IL17A* expression. Data represent mean±SE. (D) A model of increased methylation induction in IM by *H. pylori* infection. Epithelial cells with IM had markedly increased *NOS2* expression due to chromatin opening of its promoter region and enhancer reprograming, and the increased *NOS2* expression accelerated DNA methylation induction. NF-κB, nuclear factor kappa B.

expression using intestine-derived and stomach-derived organoids. Among the mouse organoids, IL-17A upregulated *NOS2* expression very potently in those from the small intestine and the colon, and moderately in those from the stomach (figure 7A left). In human organoids, IL-17A upregulated *NOS2* expression in those from the small intestine, but not in those from the stomach (figure 7a right). Importantly, IM-derived organoids showed *NOS2* induction by the treatment, while non-IM-derived organoids showed no *NOS2* induction (figure 7B). IL-17A is known to be secreted from T helper 17 cells by extracellular bacterial infection, and the mucosal biopsy samples with current *H. pylori* infection indeed showed high *IL17A* expression (figure 7C). Thus, *H. pylori* infection was considered to upregulate *NOS2* expression through IL-17A signalling in IM, and to accelerate aberrant DNA methylation induction.

## DISCUSSION

Our study provided insights at the cellular level on the long-standing question whether IM itself is a precancerous or

paracancerous lesion. First, IM crypts had a unique DNA methylation profile, namely epigenetic footprint, and the profile was present in GC more frequently than expected from the proportion of IM cells in the background mucosa. Second, IM cells suffer from accelerated induction of aberrant DNA methylation, namely epigenetic instability, likely due to increased *NOS2* expression and resultant increased DNMT activity. Taken together, IM cells were likely to have a higher chance of converting into cancer cells than non-IM cells with increased chance of gaining epigenetic alterations, supporting the precancerous nature of IM cells.

The unique DNA methylation profile of IM had similarity to that of small intestinal crypts, which was consistent with their similarity in histopathology. In addition, *CDX2*, a master regulator of the intestine,[46] and *ASCL2*, a gene reported to control intestinal stem cell fate,[47] were unmethylated in IM and small intestinal crypts, but partially methylated in non-IM crypts (online supplemental table S5), suggesting that the genes might have been demethylated to be expressed or crypts without their methylation might have been selected. Also, IM crypts showed extensive hypermethylation in promoter CGIs, including those of tumour-suppressor genes, such as *CDKN2A* and *SFRP1*. Also, genes downstream in the *TP53* pathway, such as *MIR34B*, *RPRM* and *IGFBP7*, were methylated (figure 1E), possibly leading to attenuated function of TP53 in IM cells, although IM mucosa had rare *TP53* mutations.[3 6] The lack of specific motif in TSS methylated in IM (online supplemental table S4) suggested that such regions were mainly determined by their original epigenetic status. To note, the higher levels of methylation-silencing in IM crypts also supported their precancerous nature.

The GC samples were classified into IM type and non-IM type using IM-specific methylation markers. There was no difference in the distribution of intestinal-type and diffuse-type cancers (p=0.57) (online supplemental table S7). On the other hand, regarding molecular subtype, the non-IM-type GCs mainly consisted of the chromosomal instability (CIN) type, and the IM-type GCs contained the majority of Epstein-Barr virus (EBV), MSI and genomically stable (GS) types (online supplemental table S8). Patients with IM-type GC had better survival after chemotherapy (figure 2E). This was supported by in vitro experiments using two IM cell-derived and two GC cell lines (online supplemental figure S4B), and the high composition of EBV, MSI and GS types might have been involved. Although genes involved in the sensitivity need to be isolated, such genes may provide targets for better responses to chemotherapy.[48]

The accelerated induction of aberrant DNA methylation in IM cells was indicated. We previously reported that downregulation of *TET* by microRNA through NF-κB signalling and increased DNMT activity by NO, through the nitrosation of cysteine residues of DNMT protein,[49] can induce aberrant DNA methylation in epithelial cells exposed to inflammation.[50] In this study, epithelial cells with IM had markedly increased *NOS2* expression. Although decreased expression of *TET*s was not clear, the increased *NOS2* expression was able to accelerate DNA methylation induction in at least two cell types (figure 7D). Collectively, induction of aberrant DNA methylation in IM cells was likely to be accelerated compared with gastric cells, supporting the precancerous nature of IM.

Abnormal expression of *NOS2* was induced by epigenetic alterations of histone modification and nucleosome positioning in IM. In addition, the IM mucosa samples underwent dynamic enhancer reprogramming in the *NOS2* upstream region. Also, IM cells had open chromatin in the *NOS2* enhancer region and in the *NOS2* promoter region. Notably, all types of gastric and immune cells had closed chromatin in the *NOS2* promoter region. This result showed that *NOS2* was mainly expressed in epithelial cells with IM rather than gastric or immune cells, which was in accordance with the previous reports that human macrophages showed very low expression compared with mouse macrophages.[51 52] Besides, *NOS2* expression was upregulated by IL-17A, a cytokine secreted by extracellular bacterial infection, only in IM-derived organoids, indicating that *H. pylori* infection can induce more *NOS2* expression through IL-17A signalling in IM cells. *IL17A* expression is known to be induced in the colon by specific microbiome exposure or inflammation,[45] and methylation induction may be accelerated also in the colon.[53]

Single-cell ATAC-seq is a powerful tool to explore cellular heterogeneity.[54 55] IM-pit cells were annotated by their specific genes, such as *CDX2* (figure 6B). Also, IM-pit cells were grouped with gastric pit cells, gastric mucous neck cells and gastric chief cells, which was consistent with the dysdifferentiation of IM cells from gastric cells,[56] while endocrine cells and parietal cells were isolated individually, suggesting distances in their differentiation. Although we explored the origin of IM cells using trajectory analysis (online supplemental figure S9), we were unable to infer it potentially due to the lack of cells in intermediate status. Besides, IM-pit cells were shown to contain those with *NOS2* expression, and had frequent closed chromatin of tumour-suppressor genes, including *RPRM*, *MIR34B*, *SFRP1*, *BNIP3* and *IGFBP7*, which supported the presence of aberrant DNA methylation in the IM-pit cells (online supplemental figure S8). Conversely, *CDKN2A* gained open chromatin despite the increase of its methylation level, and this was considered to be due to increased transcription in the IM-pit cells without *CDKN2A* methylation.

There are some limitations to our study and a need for future studies. First, the small number of the samples, due to the time-consuming procedures of crypt isolation by Alcian blue staining, limited the statistical power in the evaluation of IM-specific methylation profiles. The high correlation between IM-crypt samples from different individuals showed that similar epigenetic events take place in IM-crypts of different individuals. Second, the experimental periods of *NOS2* induction in normal cells, which were common in mouse experiments, were too short to mimic the human life span. Third, the analysis of histone modification used bulk IM mucosa, so that other methods of pure IM crypt purification, which do not affect the efficacy of immunoprecipitation, or single cell analysis[57 58] will be needed for more detailed analysis. Fourth, we were unable to eliminate the effect of chemotherapy or radiotherapy on methylation profiles of GC samples since no information on neoadjuvant therapy or radiation therapy before sample collection was available.

In conclusion, IM cells were considered to have a precancerous nature with an increased chance of converting into cancer cells, and an accelerated DNA methylation induction due to abnormal *NOS2* expression.

**Author affiliations**
[1]Division of Epigenomics, National Cancer Center Research Institute, Chuo-ku, Tokyo, Japan
[2]Department of Epigenomics, Institute for Advanced Life Sciences, Hoshi University, Shinagawa-ku, Tokyo, Japan
[3]Department of Gastroenterology, Graduate School of Medicine, The University of Tokyo, Bunkyo-ku, Tokyo, Japan
[4]Department of Biotechnology, Maebashi Institute of Technology, Maebashi, Gunma, Japan
[5]Gastroenterology Medicine Center, Shonan Kamakura General Hospital, Kamakura, Kanagawa, Japan
[6]Department of Gastroenterology, Faculty of Medicine, Oita University, Oita, Oita, Japan

[7]Department of Diagnostic Pathology, National Cancer Center Hospital, Chuo-ku, Tokyo, Japan
[8]Department of Gastric Surgery, National Cancer Center Hospital, Chuo-ku, Tokyo, Japan
[9]Division of Molecular Pharmacology, National Cancer Center Research Institute, Chuo-ku, Tokyo, Japan
[10]Center for Epidemiology and Preventive Medicine, The University of Tokyo Hospital, Bunkyo-ku, Tokyo, Japan

**Acknowledgements** Sample collection was supported by the National Cancer Center Biobank, Tokyo, Japan.

**Contributors** Conception and design: CT, SY and TU. Development of methodology: CT, SY, Y-YL, HT and MF. Collecting clinical samples: CT, AS, TH, TN, KI, SS, TY and AH. Acquisition of data: CT, Y-YL and HT. Analysis and interpretation of data: CT, Y-YL and TU. Writing and review of the manuscript: CT, NY, MF and TU.

**Funding** This research was supported by AMED-CREST [JP23gm1310006], AMED [JP23ck0106804], and JSPS KAKENHI [21K15941].

**Competing interests** None declared.

**Patient and public involvement** Patients and/or the public were not involved in the design, or conduct, or reporting, or dissemination plans of this research.

**Patient consent for publication** Consent obtained directly from patient(s).

**Ethics approval** This study was approved by the Institutional Review Boards of the National Cancer Center (2018-024) and the University of Tokyo (2019173G). Participants gave informed consent to participate in the study before taking part.

**Provenance and peer review** Not commissioned; externally peer reviewed.

**Data availability statement** Data are available in a public, open access repository. The data of DNA methylation (accession #GSE220511; https://www.ncbi.nlm.nih.gov/geo/query/acc.cgi?acc=GSE220511),[29] ChIP-seq (accession #GSE220681; https://www.ncbi.nlm.nih.gov/geo/query/acc.cgi?acc=GSE220681)[39] and single-cell ATAC-seq (accession #GSE221292; https://www.ncbi.nlm.nih.gov/geo/query/acc.cgi?acc=GSE221292)[43] are deposited in the Gene Expression Omnibus database (GEO) database. Genome-wide DNA methylation profiles of small intestinal crypts (accession #GSE141254; https://www.ncbi.nlm.nih.gov/geo/query/acc.cgi?acc=GSE141254),[18] blood cells (accession #GSE35069; https://www.ncbi.nlm.nih.gov/geo/query/acc.cgi?acc=GSE35069),[19] biopsy samples (accession #GSE103186; https://www.ncbi.nlm.nih.gov/geo/query/acc.cgi?acc=GSE103186),[20] human cell lines (accession #GSE68379; https://www.ncbi.nlm.nih.gov/geo/query/acc.cgi?acc=GSE68379),[21] primary gastric cancers and the corresponding adjacent mucosa (accession #GSE127857; https://www.ncbi.nlm.nih.gov/geo/query/acc.cgi?acc=GSE127857, and #GSE164988; https://www.ncbi.nlm.nih.gov/geo/query/acc.cgi?acc=GSE164988)[22 23] were obtained from the GEO. Single-cell RNA-seq data of IM mucosa samples (accession #GSE134520; https://www.ncbi.nlm.nih.gov/geo/query/acc.cgi?acc=GSE134520)[24] was obtained from the GEO.

**ORCID iDs**
Shigeki Sekine http://orcid.org/0000-0003-0884-8981
Toshikazu Ushijima http://orcid.org/0000-0003-3405-7817

## REFERENCES

1 de Vries AC, van Grieken NCT, Looman CWN, *et al*. Gastric cancer risk in patients with Premalignant gastric lesions: a nationwide cohort study in the Netherlands. *Gastroenterology* 2008;134:945–52.
2 Correa P. Human gastric carcinogenesis: a Multistep and Multifactorial process--first American Cancer society award lecture on cancer epidemiology and prevention. *Cancer Res* 1992;52:6735–40.
3 Huang KK, Ramnarayanan K, Zhu F, *et al*. Genomic and Epigenomic profiling of high-risk intestinal Metaplasia reveals molecular determinants of progression to gastric cancer. *Cancer Cell* 2018;33:137–50.
4 Schneider BG, Peng D-F, Camargo MC, *et al*. Promoter DNA Hypermethylation in gastric biopsies from subjects at high and low risk for gastric cancer. *Int J Cancer* 2010;127:2588–97.
5 Saito A, Shimoda T, Nakanishi Y, *et al*. Histologic heterogeneity and Mucin Phenotypic expression in early gastric cancer. *Pathol Int* 2001;51:165–71.
6 Kumagai K, Shimizu T, Takai A, *et al*. Expansion of gastric intestinal Metaplasia with copy number aberrations contributes to field Cancerization. *Cancer Res* 2022;82:1712–23.
7 Stachler MD, Camarda ND, Deitrick C, *et al*. Detection of mutations in Barrett's esophagus before progression to high-grade dysplasia or adenocarcinoma. *Gastroenterology* 2018;155:156–67.
8 Leedham SJ, Graham TA, Oukrif D, *et al*. Clonality, founder mutations, and field Cancerization in human ulcerative colitis-associated Neoplasia. *Gastroenterology* 2009;136:542–50.
9 Maekita T, Nakazawa K, Mihara M, *et al*. High levels of aberrant DNA methylation in Helicobacter Pylori-infected gastric Mucosae and its possible association with gastric cancer risk. *Clin Cancer Res* 2006;12(3 Pt 1):989–95.
10 Niwa T, Tsukamoto T, Toyoda T, *et al*. Inflammatory processes triggered by Helicobacter Pylori infection cause aberrant DNA methylation in gastric epithelial cells. *Cancer Res* 2010;70:1430–40.
11 Perri F, Cotugno R, Piepoli A, *et al*. Aberrant DNA methylation in non-neoplastic gastric mucosa of H. Pylori infected patients and effect of eradication. *Am J Gastroenterol* 2007;102:1361–71.
12 Asada K, Nakajima T, Shimazu T, *et al*. Demonstration of the usefulness of epigenetic cancer risk prediction by a Multicentre prospective cohort study. *Gut* 2015;64:388–96.
13 Maeda M, Nakajima T, Oda I, *et al*. High impact of methylation accumulation on Metachronous gastric cancer: 5-year follow-up of a Multicentre prospective cohort study. *Gut* 2017;66:1721–3.
14 Grady WM, Yu M, Markowitz SD. Epigenetic alterations in the gastrointestinal tract: current and emerging use for biomarkers of cancer. *Gastroenterology* 2021;160:690–709.
15 Okugawa Y, Grady WM, Goel A. Epigenetic alterations in colorectal cancer: emerging biomarkers. *Gastroenterology* 2015;149:1204–25.
16 Cancer Genome Atlas Research Network. Comprehensive molecular characterization of gastric adenocarcinoma. *Nature* 2014;513:202–9.
17 Latham A, Srinivasan P, Kemel Y, *et al*. Microsatellite instability is associated with the presence of Lynch syndrome Pan-cancer. *J Clin Oncol* 2019;37:286–95.
18 Lewis SK, Nachun D, Martin MG, *et al*. DNA methylation analysis Validates Organoids as a viable model for studying human intestinal aging (methylation) [Gene Expression Omnibus]. 2020. Available: https://www.ncbi.nlm.nih.gov/geo/query/acc.cgi?acc=GSE141254
19 Reinius LA, Joerink N, Pershagen, M. Differential DNA methylation in purified human blood cells [Gene Expression Omnibus]. 2019. Available: https://www.ncbi.nlm.nih.gov/geo/query/acc.cgi?acc=GSE35069
20 Huang K, Patrick T. Genomic and Epigenomic profiling of high-risk intestinal Metaplasia reveals molecular determinants of gastric cancer progression [Gene Expression Omnibus]. 2021. Available: https://www.ncbi.nlm.nih.gov/geo/query/acc.cgi?acc=GSE103186
21 Moran S, Heyn H, Esteller M. The landscape of Pharmacogenomic interactions in human cancer [Gene Expression Omnibus]. 2019. Available: https://www.ncbi.nlm.nih.gov/geo/query/acc.cgi?acc=GSE68379
22 Berdasco M. DNA methylation profiling of gastric cancer and precursor lesions [Gene Expression Omnibus]. 2021. Available: https://www.ncbi.nlm.nih.gov/geo/query/acc.cgi?acc=GSE127857
23 Ghosh S, Lamare F. Identification and development of DNA methylation biomarkers for stomach cancers prevalent in Mizoram, India [Gene Expression Omnibus]. 2021. Available: https://www.ncbi.nlm.nih.gov/geo/query/acc.cgi?acc=GSE164988
24 Li S, Zhang P. Dissecting the single-cell Transcriptome network underlying gastric Premalignant lesions and early gastric cancer 10X Genomics [Gene Expression Omnibus]. 2021. Available: https://www.ncbi.nlm.nih.gov/geo/query/acc.cgi?acc=GSE134520
25 Takeuchi C, Sato J, Yamashita S, *et al*. Autoimmune Gastritis induces aberrant DNA methylation reflecting its carcinogenic potential. *J Gastroenterol* 2022;57:144–55.
26 Iida N, Okuda Y, Ogasawara O, *et al*. MACON: a web tool for computing DNA methylation data obtained by the Illumina Infinium human DNA methylation Beadarray. *Epigenomics* 2018;10:249–58.
27 Yamada H, Takeshima H, Fujiki R, *et al*. Arid1A loss-of-function induces CpG Island Methylator phenotype. *Cancer Lett* 2022;532:215587.
28 Zong L, Hattori N, Yoda Y, *et al*. Establishment of a DNA methylation marker to evaluate cancer cell fraction in gastric cancer. *Gastric Cancer* 2016;19:361–9.
29 Takeuchi C, Yamashita S, Ushijima T. Genome-wide DNA methylation analysis using gastric crypts with intestinal Metaplasia and NOS2-inducible cell lines [Gene Expression Omnibus]. 2022. Available: https://www.ncbi.nlm.nih.gov/geo/query/acc.cgi?acc=GSE220511
30 Doi A, Park I-H, Wen B, *et al*. Differential methylation of Tissue- and cancer-specific CpG Island shores distinguishes human induced Pluripotent stem cells, embryonic stem cells and fibroblasts. *Nat Genet* 2009;41:1350–3.
31 Irie T, Yamada H, Takeuchi C, *et al*. The methylation level of a single cancer risk marker gene reflects methylation burden in gastric mucosa. *Gastric Cancer* 2023;26:667–76.
32 Yoda Y, Takeshima H, Niwa T, *et al*. Integrated analysis of cancer-related pathways affected by genetic and epigenetic alterations in gastric cancer. *Gastric Cancer* 2015;18:65–76.
33 Takeshima H, Niwa T, Takahashi T, *et al*. Frequent involvement of Chromatin Remodeler alterations in gastric field Cancerization. *Cancer Lett* 2015;357:328–38.
34 Ajani JA, D'Amico TA, Bentrem DJ, *et al*. Gastric cancer, version 2.2022, NCCN clinical practice guidelines in oncology. *J Natl Compr Canc Netw* 2022;20:167–92.
35 Hur K, Niwa T, Toyoda T, *et al*. Insufficient role of cell proliferation in aberrant DNA methylation induction and involvement of specific types of inflammation. *Carcinogenesis* 2011;32:35–41.

36 Katsurano M, Niwa T, Yasui Y, *et al*. Early-stage formation of an epigenetic field defect in a mouse colitis model, and non-essential roles of T- and B-cells in DNA methylation induction. *Oncogene* 2012;31:342–51.
37 Bartfeld S, Bayram T, van de Wetering M, *et al*. In vitro expansion of human gastric epithelial stem cells and their responses to bacterial infection. *Gastroenterology* 2015;148:126–36.
38 Xie W, Schultz MD, Lister R, *et al*. Epigenomic analysis of Multilineage differentiation of human embryonic stem cells. *Cell* 2013;153:1134–48.
39 Takeuchi C, Yamashita S, Liu Y, *et al*. Chip-Seq analysis of H3K27Acethylation using gastric mucosa with intestinal Metaplasia [Gene Expression Omnibus]. 2022. Available: https://www.ncbi.nlm.nih.gov/geo/query/acc.cgi?acc=GSE220681
40 Mutoh H, Hakamata Y, Sato K, *et al*. Conversion of gastric mucosa to intestinal Metaplasia in Cdx2-expressing transgenic mice. *Biochem Biophys Res Commun* 2002;294:470–9.
41 de Vera ME, Shapiro RA, Nussler AK, *et al*. Transcriptional regulation of human inducible nitric oxide synthase (NOS2) gene by Cytokines: initial analysis of the human NOS2 promoter. *Proc Natl Acad Sci U S A* 1996;93:1054–9.
42 Taylor BS, de Vera ME, Ganster RW, *et al*. Multiple NF-kappaB enhancer elements regulate cytokine induction of the human inducible nitric oxide synthase gene. *J Biol Chem* 1998;273:15148–56.
43 Takeuchi C, Yamashita S, Liu Y, *et al*. scATAC-Seq analysis using gastric mucosa with intestinal Metaplasia [Gene Expression Omnibus]. 2022. Available: https://www.ncbi.nlm.nih.gov/geo/query/acc.cgi?acc=GSE221292
44 Zhang P, Yang M, Zhang Y, *et al*. Dissecting the single-cell Transcriptome network underlying gastric Premalignant lesions and early gastric cancer. *Cell Rep* 2019;27:1934–47.
45 Nanki K, Fujii M, Shimokawa M, *et al*. Somatic inflammatory gene mutations in human ulcerative colitis epithelium. *Nature* 2020;577:254–9.
46 Silberg DG, Swain GP, Suh ER, *et al*. Cdx1 and Cdx2 expression during intestinal development. *Gastroenterology* 2000;119:961–71.
47 van der Flier LG, van Gijn ME, Hatzis P, *et al*. Transcription factor Achaete Scute-like 2 controls intestinal stem cell fate. *Cell* 2009;136:903–12.
48 Han S-W, Lee H-J, Bae JM, *et al*. Methylation and Microsatellite status and recurrence following adjuvant FOLFOX in colorectal cancer. *Int J Cancer* 2013;132:2209–16.
49 Hmadcha A, Bedoya FJ, Sobrino F, *et al*. Methylation-dependent gene silencing induced by interleukin 1Beta via nitric oxide production. *J Exp Med* 1999;190:1595–604.
50 Takeshima H, Niwa T, Yamashita S, *et al*. TET repression and increased DNMT activity synergistically induce aberrant DNA methylation. *J Clin Invest* 2020;130:5370–9.
51 Gross TJ, Kremens K, Powers LS, *et al*. Epigenetic silencing of the human NOS2 gene: Rethinking the role of nitric oxide in human macrophage inflammatory responses. *J Immunol* 2014;192:2326–38.
52 Schneemann M, Schoedon G, Hofer S, *et al*. Nitric oxide synthase is not a constituent of the antimicrobial Armature of human mononuclear phagocytes. *J Infect Dis* 1993;167:1358–63.
53 Hattori N, Niwa T, Ishida T, *et al*. Antibiotics suppress colon tumorigenesis through inhibition of aberrant DNA methylation in an Azoxymethane and dextran sulfate sodium colitis model. *Cancer Sci* 2019;110:147–56.
54 Buenrostro JD, Wu B, Litzenburger UM, *et al*. Single-cell Chromatin accessibility reveals principles of regulatory variation. *Nature* 2015;523:486–90.
55 Cusanovich DA, Daza R, Adey A, *et al*. Multiplex single cell profiling of Chromatin accessibility by Combinatorial cellular indexing. *Science* 2015;348:910–4.
56 Goldenring JR, Mills JC. Cellular plasticity, Reprogramming, and regeneration: Metaplasia in the stomach and beyond. *Gastroenterology* 2022;162:415–30.
57 Rotem A, Ram O, Shoresh N, *et al*. Single-cell chip-Seq reveals cell subpopulations defined by Chromatin state. *Nat Biotechnol* 2015;33:1165–72.
58 Grosselin K, Durand A, Marsolier J, *et al*. High-throughput single-cell chip-Seq identifies heterogeneity of Chromatin States in breast cancer. *Nat Genet* 2019;51:1060–6.

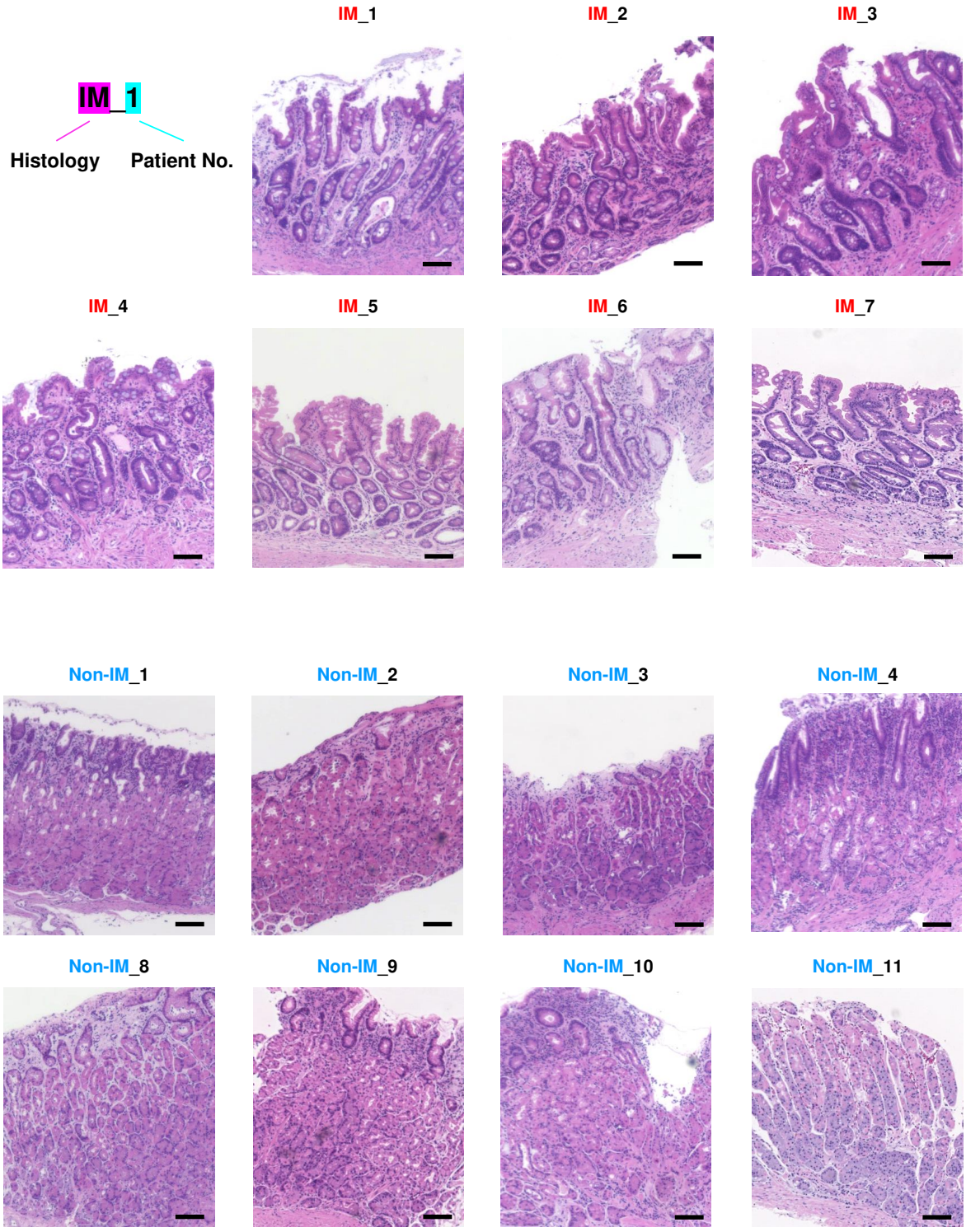
IM_1
Histology
Patient No.
IM_1
IM_2
IM_3
IM_4
IM_5
IM_6
IM_7
Non-IM_1
Non-IM_2
Non-IM_3
Non-IM_4
Non-IM_8
Non-IM_9
Non-IM_10
Non-IM_11

**Fig. S1**

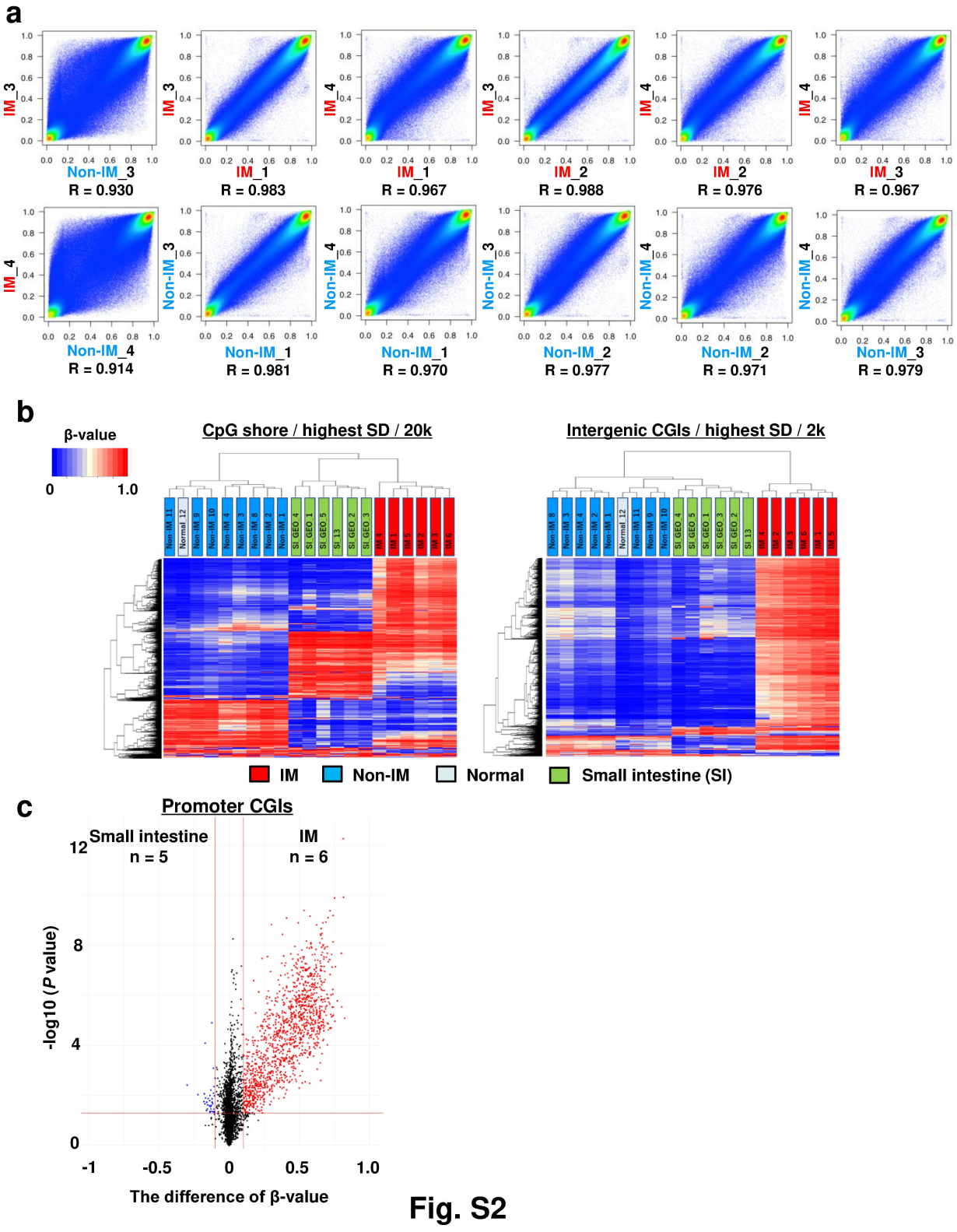
a
IM_3
Non-IM_3
R = 0.930
IM_3
IM_1
R = 0.983
IM_4
IM_1
R = 0.967
IM_3
IM_2
R = 0.988
IM_4
IM_2
R = 0.976
IM_4
IM_3
R = 0.967
IM_4
Non-IM_4
R = 0.914
Non-IM_3
Non-IM_1
R = 0.981
Non-IM_4
Non-IM_1
R = 0.970
Non-IM_3
Non-IM_2
R = 0.977
Non-IM_4
Non-IM_2
R = 0.971
Non-IM_4
Non-IM_3
R = 0.979
b
β-value
0
1.0
CpG shore / highest SD / 20k
Intergenic CGIs / highest SD / 2k
IM
Non-IM
Normal
Small intestine (SI)
c
Promoter CGIs
Small intestine
n = 5
IM
n = 6
-log10 (P value)
12
8
4
0
-1
-0.5
0
0.5
1.0
The difference of β-value

**Fig. S2**

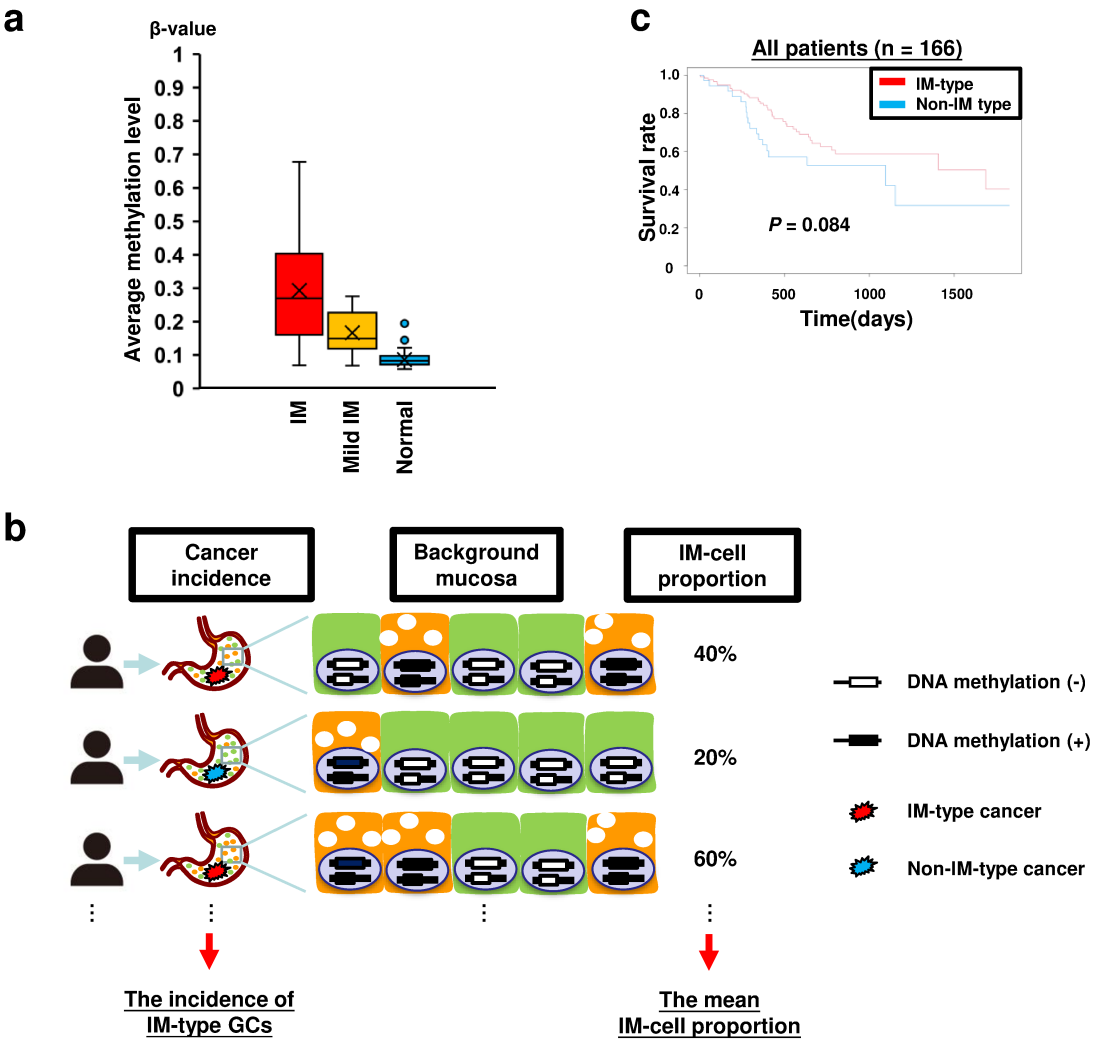
a
β-value
Average methylation level
1
0.9
0.8
0.7
0.6
0.5
0.4
0.3
0.2
0.1
0
IM
Mild IM
Normal
c
All patients (n = 166)
IM-type
Non-IM type
Survival rate
1.0
0.8
0.6
0.4
0.2
0
P = 0.084
0
500
1000
1500
Time(days)
b
Cancer incidence
Background mucosa
IM-cell proportion
40%
20%
60%
DNA methylation (-)
DNA methylation (+)
IM-type cancer
Non-IM-type cancer
The incidence of IM-type GCs
The mean IM-cell proportion

**Fig. S3**

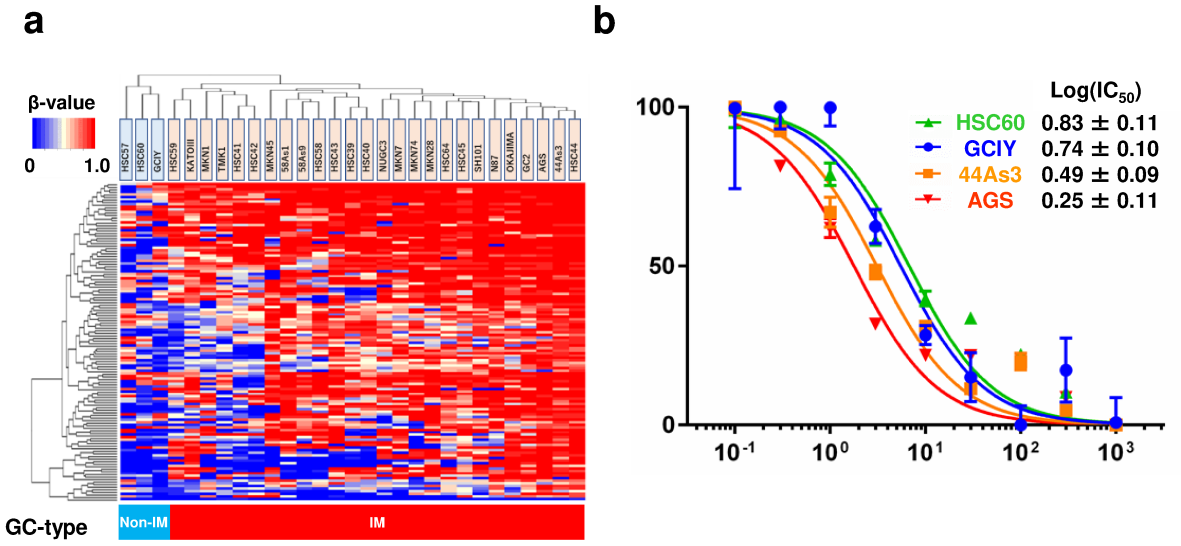
a
β-value
0
1.0
HSC57
HSC60
GCIY
HSC59
KATOIII
MKN1
TMK1
HSC41
HSC42
MKN45
S6As1
S6As9
HSC58
HSC43
HSC39
HSC40
NUGC3
MKN7
MKN74
MKN28
HSC44
HSC45
SH101
N87
OKAJIMA
GC2
AGS
44As3
HSC44
GC-type
Non-IM
IM
b
Log(IC50)
HSC60 0.83 ± 0.11
GCIY 0.74 ± 0.10
44As3 0.49 ± 0.09
AGS 0.25 ± 0.11
100
50
0
10-1
100
101
102
103

**Fig. S4**

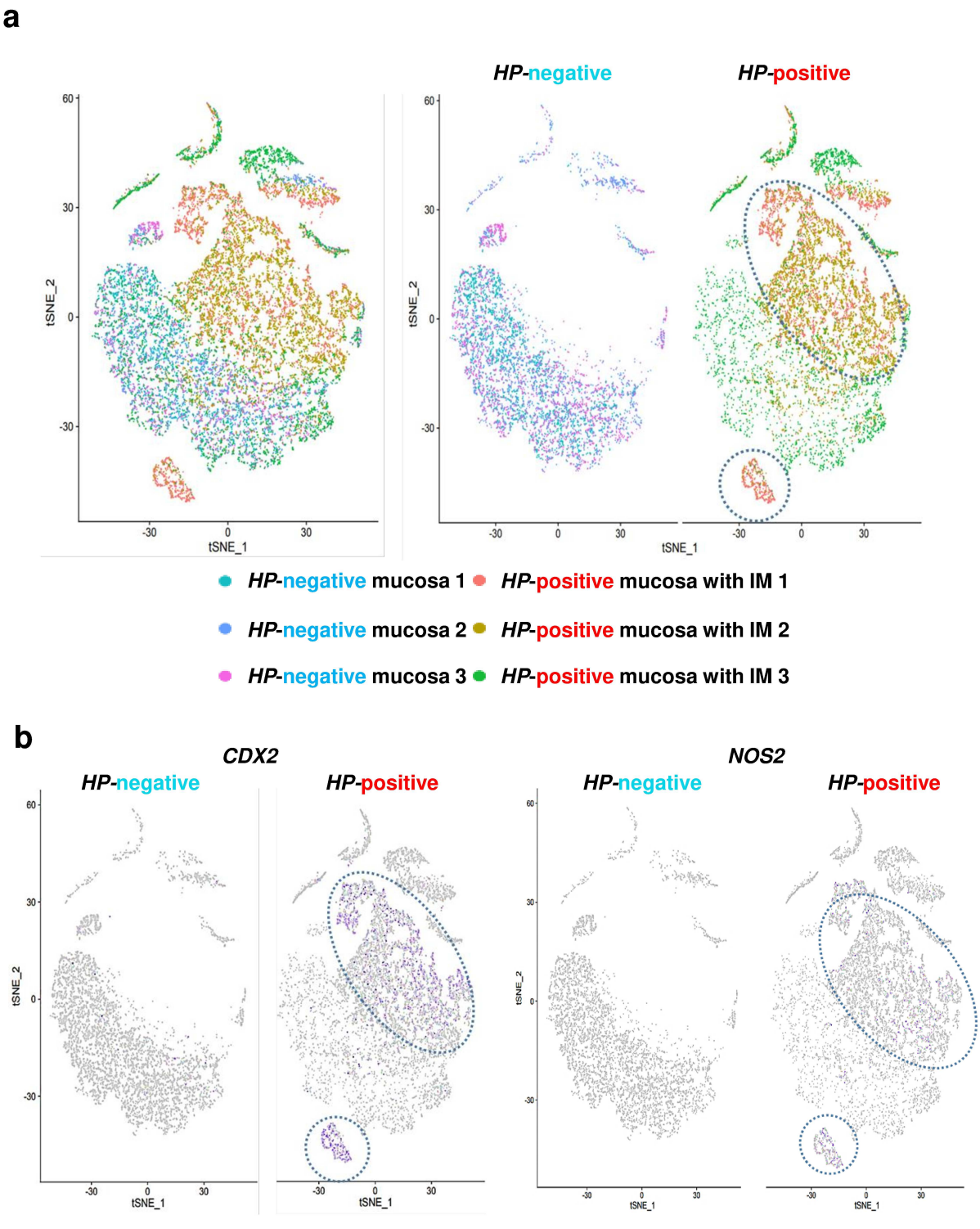
a
HP-negative
HP-positive
tSNE_1
tSNE_2
HP-negative mucosa 1
HP-positive mucosa with IM 1
HP-negative mucosa 2
HP-positive mucosa with IM 2
HP-negative mucosa 3
HP-positive mucosa with IM 3
b
CDX2
NOS2
HP-negative
HP-positive

**Fig. S5**

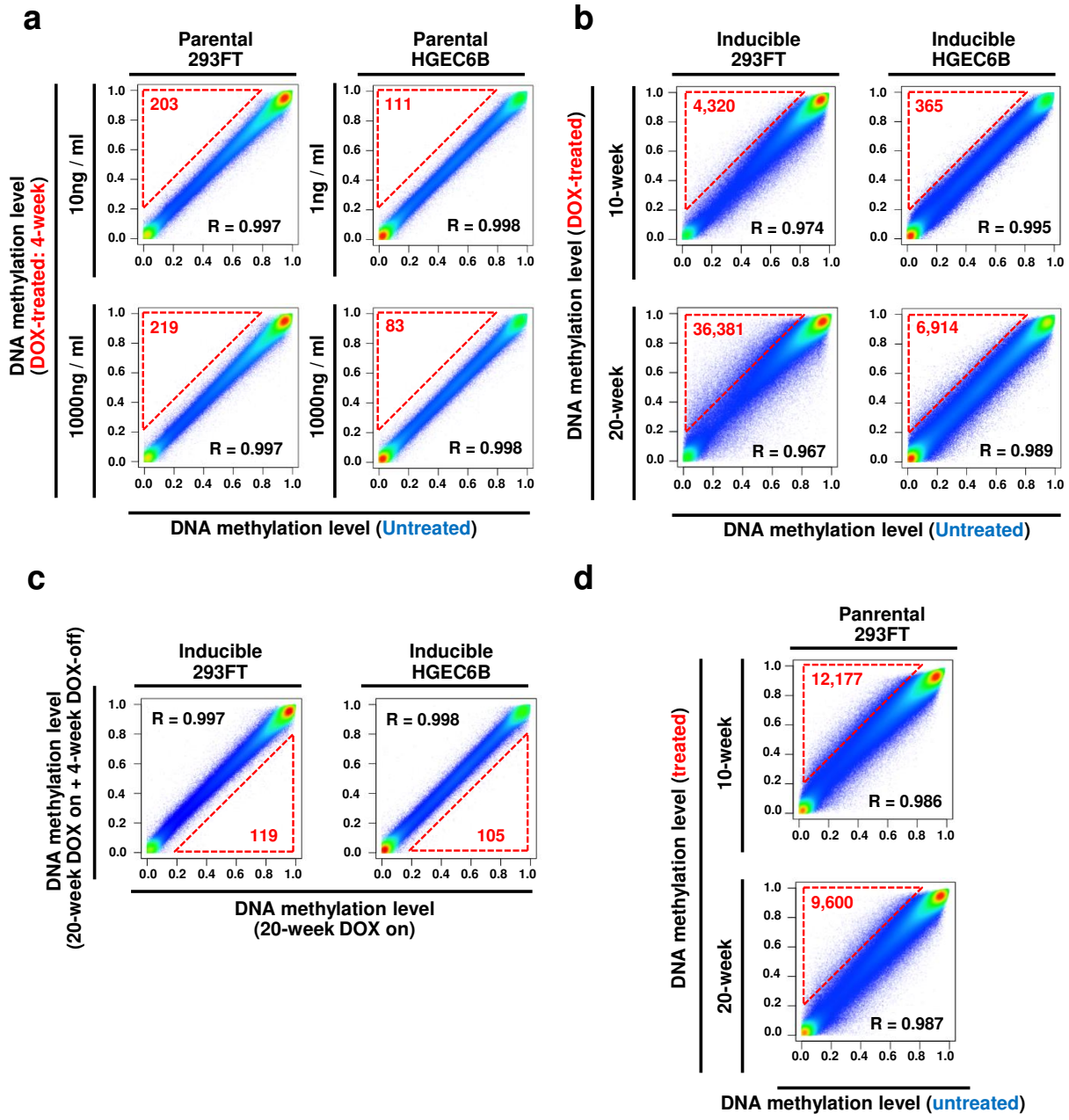
a
Parental 293FT
Parental HGEC6B
DNA methylation level (DOX-treated: 4-week)
10ng / ml
1ng / ml
1000ng / ml
1000ng / ml
203
111
219
83
R = 0.997
R = 0.998
R = 0.997
R = 0.998
DNA methylation level (Untreated)
b
Inducible 293FT
Inducible HGEC6B
DNA methylation level (DOX-treated)
10-week
20-week
4,320
365
36,381
6,914
R = 0.974
R = 0.995
R = 0.967
R = 0.989
DNA methylation level (Untreated)
c
Inducible 293FT
Inducible HGEC6B
DNA methylation level (20-week DOX on + 4-week DOX-off)
R = 0.997
R = 0.998
119
105
DNA methylation level (20-week DOX on)
d
Panrental 293FT
DNA methylation level (treated)
10-week
20-week
12,177
9,600
R = 0.986
R = 0.987
DNA methylation level (untreated)

**Fig. S6**

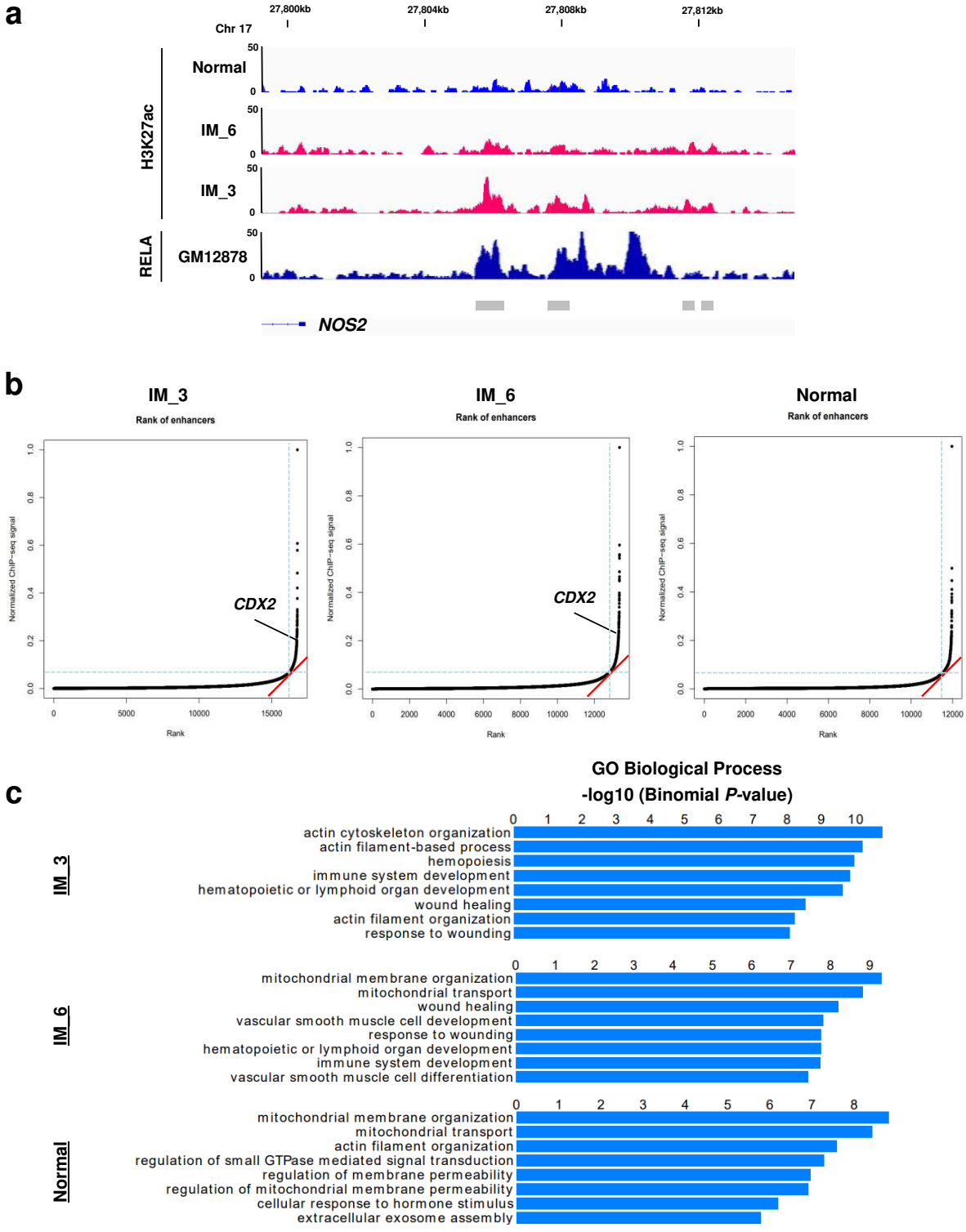
a
27,800kb
27,804kb
27,808kb
27,812kb
Chr 17
H3K27ac
Normal
IM_6
IM_3
RELA
GM12878
NOS2
b
IM_3
IM_6
Normal
Rank of enhancers
Normalized ChIP-seq signal
Rank
CDX2
c
GO Biological Process
-log10 (Binomial P-value)
IM_3
actin cytoskeleton organization
actin filament-based process
hemopoiesis
immune system development
hematopoietic or lymphoid organ development
wound healing
actin filament organization
response to wounding
IM_6
mitochondrial membrane organization
mitochondrial transport
wound healing
vascular smooth muscle cell development
response to wounding
hematopoietic or lymphoid organ development
immune system development
vascular smooth muscle cell differentiation
Normal
mitochondrial membrane organization
mitochondrial transport
actin filament organization
regulation of small GTPase mediated signal transduction
regulation of membrane permeability
regulation of mitochondrial membrane permeability
cellular response to hormone stimulus
extracellular exosome assembly

**Fig. S7**

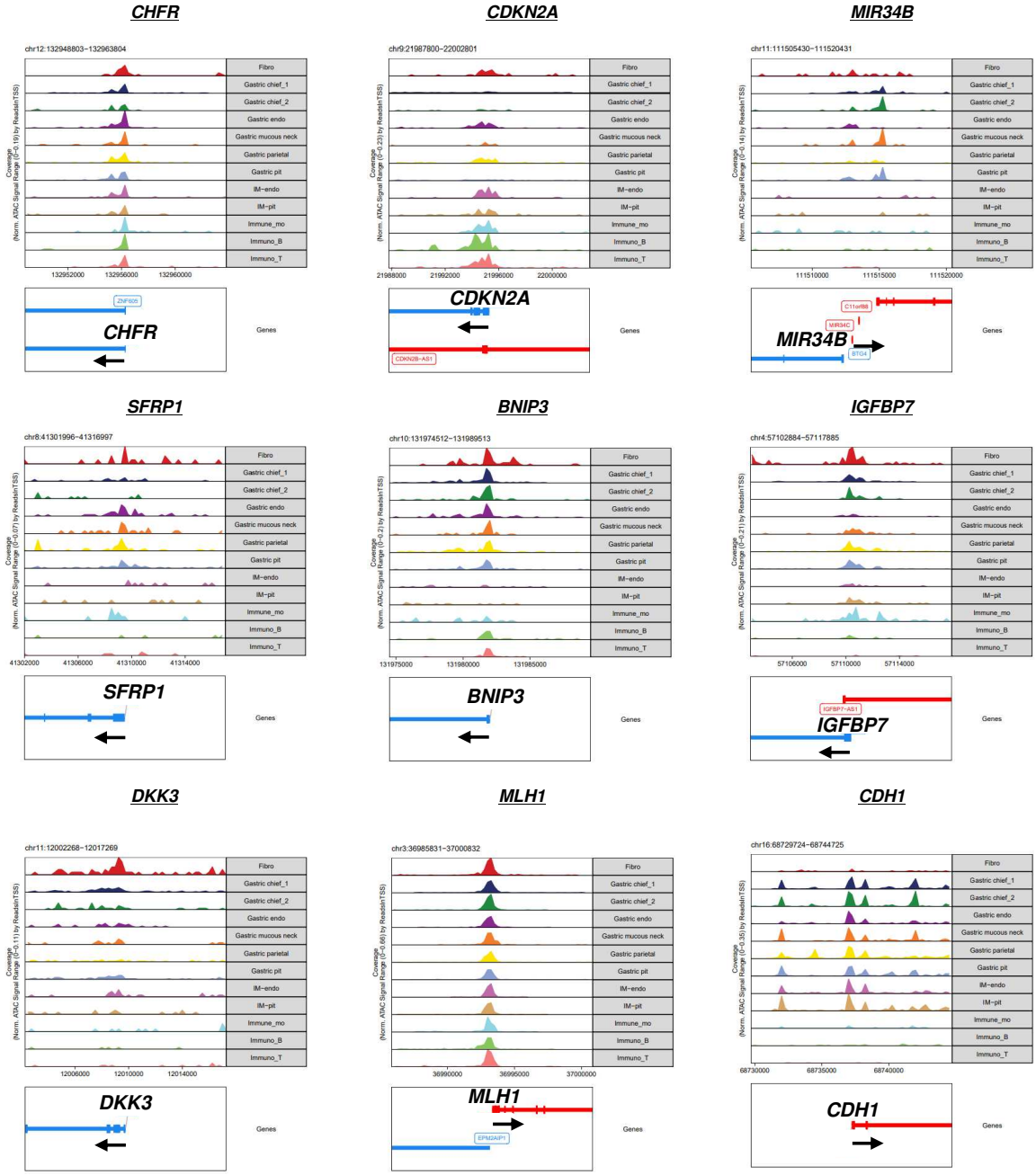
CHFR
CDKN2A
MIR34B
SFRP1
BNIP3
IGFBP7
DKK3
MLH1
CDH1
Fibro
Gastric chief_1
Gastric chief_2
Gastric endo
Gastric mucous neck
Gastric parietal
Gastric pit
IM−endo
IM−pit
Immune_mo
Immuno_B
Immuno_T
Genes

**Fig. S8**

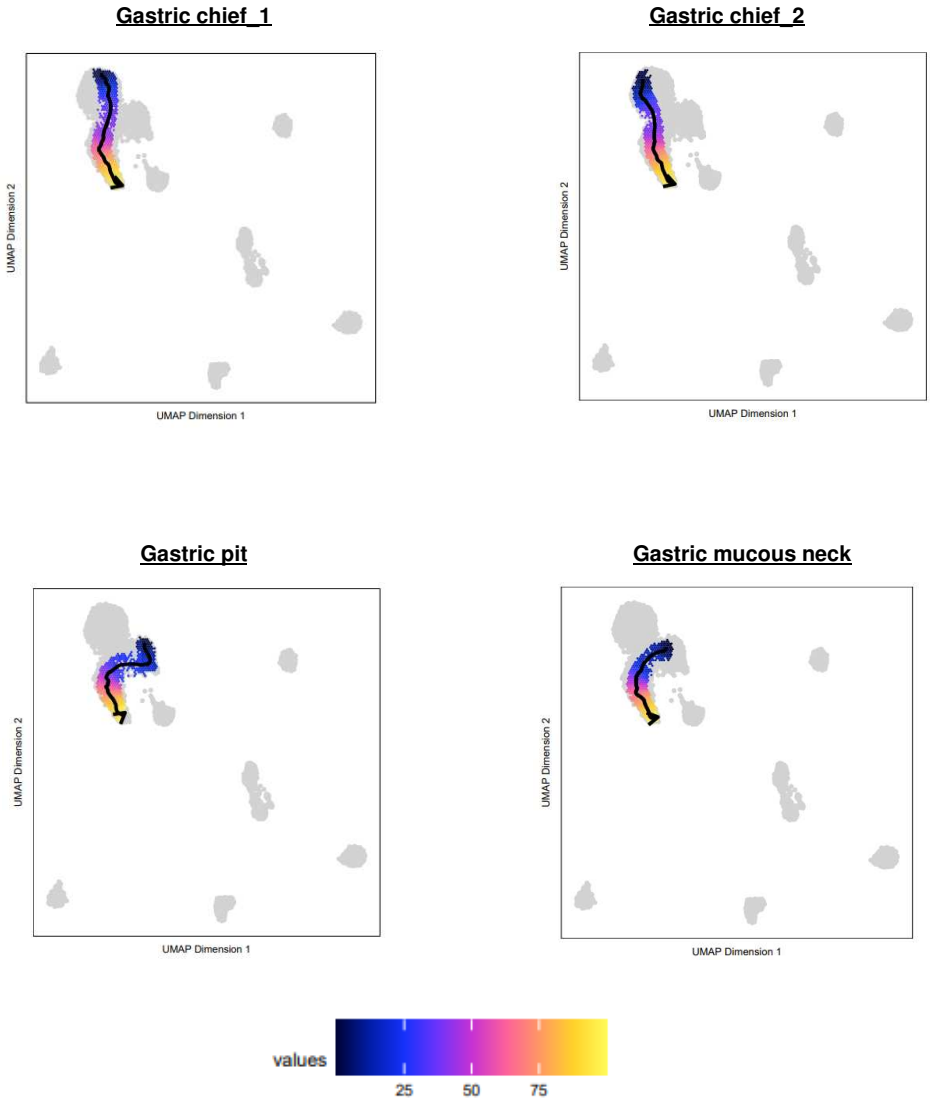
Gastric chief_1
Gastric chief_2
Gastric pit
Gastric mucous neck
UMAP Dimension 1
UMAP Dimension 2
values
25
50
75

**Fig. S9**

# Supplementary Methods

### *Crypt isolation and DNA extraction*

Gastric and intestinal crypts were freshly isolated from gastric and intestinal mucosa, respectively, by incubating them at 37°C in calcium- and magnesium-free Hanks' balanced salt solution with 30 mM EDTA for 30 min with gentle shaking, and crypts were scraped off with the dorsal side of a scalpel and fixed in 70% ethanol. Isolated crypts were stained with an Alcian Blue Stain Kit (Abcam, Cambridge, UK) to distinguish IM crypts from non-IM crypts, and the crypts positive for staining of goblet cells were considered as IM crypts. 100 to 500 crypts were collected under microscopy for DNA extraction by the phenol and chloroform extraction method.

### *Mucosal biopsy*

All the gastric mucosa samples were endoscopically biopsied from the greater curvature in the middle corpus region and were stored in RNAlater (Thermo Fisher Scientific, MA, USA) at −80°C until further use.

### *Genome-wide DNA methylation analysis*

From the 862,927 probes of CpG sites, 843,393 probes located on autosomes were used for analysis. The 843,393 probes on autosomes were assembled into 535,685 genomic blocks, a collection of probes according to their locations against transcription start sites (TSSs) and CpG islands (CGIs) [1]. The target CpG sites of the genomic blocks corresponding to tumor-suppressor genes (*CHFR*, *CDKN2A*, *RPRM*, *miR-34b*, *SFRP1*, *BNIP3*, *IGFBP7*, *DKK3, MLH1* and *CDH1*) [2, 3, 4, 5] and risk marker genes (*miR-124a-3*, *EMX1* and *NKX6-1*) [6, 7] are listed in Table S11.

***Pathway enrichment analysis***

Pathway enrichment analysis was conducted by DAVID (https://david.ncifcrf.gov/summary.jsp) using the KEGG_PATHWAY gene sets [8].

***Motif analysis***

Motif analysis using differentially methylated promoter CGIs was conducted by HOMER (http://homer.ucsd.edu/homer/index.html) [9] with default parameters.

***Kaplan-Meier plotting analysis***

Publicly available TCGA (The Cancer Genome Atlas) data sets at the GDC data portal (https://portal.gdc.cancer.gov/) were used to plot overall survival curves of gastric cancer patients using R 4.0.5 with the survival package. According to the log-rank test, *P*-values $< 0.05$ were considered statistically significant.

***Cell culture***

293FT cells was purchased from Thermo Fisher Scientific (MA, USA), GCIY cells from RIKEN BioResource Center Cell Bank (Ibaraki, Japan), and AGS and Caco-2 cells from the American Type Culture Collection (ATCC, VA, USA). 44As3 and HSC60 cells were kindly provided by Dr. K. Yanagihara at the National Cancer Center and HGEC6B cells by Dr. T. Kiyono at the National Cancer Center. The cells were cultured in Roswell Park Memorial Institute (RPMI)-1640 (AGS, 44As3, and HSC60), Dulbecco's modified Eagle medium (DMEM) with high glucose (293FT, GCIY, and Caco-2) or Keratinocyte-SFM (HGEC6B) at 37 °C in a humidified atmosphere with 5% CO2. All media were supplemented with 10% fetal bovine serum and 1% penicillin/streptomycin (Thermo Fisher Scientific). The cells were tested for Mycoplasma infection using the MycoAlert mycoplasma detection kit (Lonza, Basel, Switzerland).

***Drug sensitivity assay***

For the sensitivity assay to cytotoxic drugs, the cells (GCIY, 44As3, HSC60, and AGS) were seeded at a density of $2 \times 10^3$ cells per well in a 96-well microplate on day 0 in triplicate. The cells were treated with 5-FU on day 1 for 72 h, and cell viability was evaluated using a WST-8 assay (Nacalai tesque, Kyoto, Japan) on day 4. Briefly, each well was added with 10 µl of WST-8 and incubated for 2 h at 37 °C. The absorbance of each sample was determined using a microplate reader (Wallac 1420 Victor2, PerkinElmer, MA, USA) with a reference wavelength of 450 nm. The average of the triplicate values was normalized against that of untreated cells. The half-maximal inhibitory concentration ($IC_{50}$) and a 95%-confidence interval were calculated by the non-linear regression analysis of log (inhibitor) versus the normalized response with a variable slope using a GraphPad Prism program (GraphPad Software, CA, USA).

***Quantitative real-time RT-PCR***

Total RNA of gastric biopsy samples was extracted using RNeasy Mini Kit (Qiagen, CA, USA). Reverse transcription was performed using Superscript IV Reverse Transcriptase (Thermo Fisher Scientific). Quantitative RT-PCR was performed with CFX connect Real-Time Detection System (Bio-Rad, CA, USA) using SYBR Green I (Lonza, Basel, Switzerland) and AmpliTaq Gold Polymerase (Thermo Fisher Scientific). A copy number of a gene transcript was obtained by comparison of its amplification curve to those of standard DNA samples with known copy numbers, and was normalized to that of *GAPDH*. The primer sequences for target genes are shown in Table S12.

***Data analysis of single-cell RNA-seq***

The sequencing data using the gastric mucosa were obtained from the GEO (accession #GSE134520) [10]. The data of *H. pylori*-negative mucosa samples (n = 3) and positive mucosa samples with IM (n = 3) were analyzed using Seurat (v4.0.2) [11] R package. The cells with high quality reads (nFeature_RNA > 200 & nFeature_RNA < 2500 &

percent.mt < 5) were used for further analysis. Data normalization was performed by NormalizeData with setting normalization method as LogNormalize. Genes with large variations were selected by FindVariableFeatures with default parameters. Data scaling was performed by ScaleData with default parameters. Dimension reduction was performed by RunPCA with default parameters to draw a tSNE plot. Clustering was performed using FindNeighbors and FindClusters with default parameters before t-SNE dimensional reduction.

***Immunohistochemistry***

Gastric mucosa from a resected specimen was freshly obtained and paraffin-embedded after formalin fixation. Sections of 5-μm thickness were prepared, and deparaffinization, rehydration, and endogenous peroxidase inactivation of the sections were performed following standard procedures. Thereafter heat-induced epitope retrieval was performed in citrate buffered solution pH 6.0 (Kanto Chemical, Tokyo, Japan) in an autoclave for 15 minutes. The sections were incubated with rabbit anti-iNOS (PA1-036, Invitrogen, MA, USA) antibody for 16 h at room temperature, followed by the treatment with EnVision/FLEX HRP (Dako, CA, USA). The sections were visualized in 20 mg/dl 3,3'-diaminobenzidine (DAB).

***Organoid establishment and culture***

Human-derived organoids were established from gastric and small intestinal mucosa from resected specimen as previously described [12]. Briefly, obtained gastric mucosa were minced with a scalpel. They were incubated vigorously in dissociation buffer [advanced DMEM/F-12 medium (Thermo Fisher Scientific) with 1x GlutaMAX (Thermo Fisher Scientific), 10mM HEPES (Thermo Fisher Scientific), 2mg/ml BSA (Sigma-Aldrich, MA, USA) and 1mg/ml collagenase (Thermo Fisher Scientific)] at 37°C for 45 min. After filtration and repeated washing, isolated glands were seeded in Matrigel (Corning, NY, USA) and cultured in basal medium [advanced DMEM/F-12 medium with

10 mM HEPES, 1x GlutaMAX, 1× B27 (Thermo Fisher Scientific), 1mM *N*-acetyl-L-cysteine (FUJIFILM Wako, Tokyo, Japan), 1x penicillin/streptomycin and 1x amphotericin B (Thermo Fisher Scientific)] supplemented with L-WRN conditioned medium (CM) [13], gastrin (Sigma-Aldrich), EGF (Thermo Fisher Scientific), CHIR99021 (Sigma-Aldrich), A83-01 (Tocris Bioscience, MN, USA) and Y27632 (FUJIFILM Wako). FGF (PeproTech, NJ, USA) was supplemented only for stomach organoids.

Mouse-derived organoids were established from gastric and small intestinal mucosa from resected specimen as previously described [14]. Briefly, obtained gastric mucosa were cut into small pieces, was incubated in chelation buffer (PBS (-) with 43.4 mM sucrose and 54.9 mM D-sorbitol and 5 mM EDTA) at 4°C for 2 hour and glands was isolated by vigorous shaking. After filtration and repeated washing, isolated glands were seeded in Matrigel and cultured in basal medium (advanced DMEM/F-12 medium with 10 mM HEPES, 1x GlutaMAX, 1× N2, 1× B27, 1mM *N*-acetyl-L-cysteine, 1x penicillin/streptomycin and 1x amphotericin B) supplemented with L-WRN CM, EGF, CHIR99021, A83-01, and Y27632. Gastrin and FGF were supplemented only for gastric organoids.

Only primary organoids were used in this study. The medium was refreshed every three days and the organoids were passaged once a week. To evaluate the effect of cytokine treatment on organoids, the organoids were treated with 30 ng/ml TNF (R&D Systems, MN, USA) for 2h, 10 ng/ml IL-1B (R&D Systems) for 2h or 100 ng/ml IL-17A (PeproTech) for 24h. Total RNA of the organoids was extracted using RNeasy Mini Kit.

***Establishment of a NOS2-inducible cell line***

The vectors (pLV[TetOn]-EGFP:T2A:Puro-TRE3G>hNOS2[NM_000625.4]; VB191011-2309fwc, pLV[Exp]-CMV>Tet3G/Hygro; VB180123-1018bxq) for Tet-On 3G inducible gene expression system were purchased from VectorBuilder (IL, USA). Each vector was co-transfected with pPACK Packaging Plasmid Mix (System Biosciences) into



Takeuchi C, *et al. Gut* 2023;0:1–13. doi: 10.1136/gutjnl-2023-329492

293TN cells using Lipofectamine 3000 with Plus Reagent (Thermo Fisher Scientific). Medium containing lentivirus was collected 48 h after transfection and stored at −80°C until further use. 293FT cells and HGEC6B cells (normal human gastric epithelial cell line) were infected with each lentivirus and were selected by puromycin and hygromycin.

***DNMT activity analysis***

Nuclear proteins were extracted from *NOS2*-inducible cells (293FT) 24h after DOX treatment by an EpiQuik Nuclear Extraction Kit I (Epigentek, NY, USA). Using 10 μg nuclear protein, DNMT activity was measured by an EpiQuik DNMT Activity/Inhibition Assay Ultra Kit (Epigentek).

***Chromatin immunoprecipitation sequencing (ChIP-seq)***

Gastric mucosa from resected specimen was incubated at 37°C in calcium- and magnesium-free Hanks' balanced salt solution with 30 mmol/L EDTA for 30 min with gentle shaking. The crypts were scraped off with the dorsal side of a scalpel. Crosslinking and immunoprecipitation by anti-H3K27ac antibody (ab4729, Abcam) were performed as previously described [15]. Using 10 ng immunoprecipitated and input DNA, a sequencing library was prepared using a GeneNext NGS Library Prep Kit (TOYOBO, Osaka, Japan). DNA fragments between 150 bp and 400 bp were purified using Agencourt AMPure XP (Beckman Coulter, CA, USA) after 8 cycles of PCR amplification, and were sequenced by Illumina HiSeq-X in 150 bp paired-end mode at a final sequencing depth around 30-54 million reads. The sequencing data of GM12878 for H3K27ac were obtained from ENCODE (https://www.encodeproject.org/).

Sequencing data were aligned to the hg38 using bowtie2 (v2.4.1) [16] using default parameters. Duplicates were removed using samtools (v1.16.1). Fragment pileup at every base pair was normalized to reads per million mapped reads and was displayed with the location of peaks in the Integrative Genomics Viewer [17]. Super-enhancers were called as previously reported [18, 19]. First, peaks called by MACS2 [20] at ±2,500 bp around TSS

were excluded, and peaks at a distance smaller than 12,500 bp were stitched into a single peak. Pileup signals in each stitched peak were summed and normalized to reads per million per bp (rpm/bp), and the resultant value was used as read density. To distinguish enhancers and super-enhancers, all stitched peaks were ranked along the x-axis by the background-subtracted ChIP-seq read density in increasing order, and the threshold was the intersection of the slope of 1 tangent to the curve produced by the ranking. Peaks below and above the threshold were defined as typical enhancers or super-enhancers, respectively. Annotation of each peak was performed with UROPA [21].

Heatmaps of ChIP/input enrichment around the peaks were created from deepTools (v3.5.1) [22] using bamCompare, computeMatrix, and plotHeatmap. GREAT (v4.0.2) was used to annotate the potential functions of the peaks with default parameters [23]. A gene most proximal to a region with H3K27ac change was considered to be affected by the change. BigWig files for visualization in the Integrative Genomics Viewer (IGV) were generated by deepTools using bamCoverage with options (--binSize 10 --normalizeUsing RPGC --effectiveGenomeSize 2913022398 --ignoreForNormalization chrX --extendReads).

***Single-cell Assay for Transposase-Accessible Chromatin Sequencing (single-cell ATAC-seq)***

Nucleus was isolated from gastric mucosa stored in STEM-CELLBANKER (ZENOAQ, Fukushima, Japan) freezing medium at －80°C according to the protocol descried by 10x Genomics (CA, USA) (https://www.10xgenomics.com/support/single-cell-atac), and a library was prepared using Chromium Next GEM Single Cell ATAC Kit (v1.1) (10x Genomics). The prepared library was sequenced by Illumina HiSeq-X. Using the sequencing data, quality control and pre-processing were performed by the Cell Ranger ATAC v2.0.0. The processed files (fragments.tsv files) were analyzed using ArchR (v1.0.2) [24] R package.

Briefly, the sequencing data were aligned to the hg38. Arrow files were created using the cells retaining cell barcodes with at least 2,000 fragments and a TSS enrichment score > 6. Doublets were identified and filtered using addDoubletscores and filterDoublets (filter ratio = 2.5). LSI iterative dimension reduction was performed with default parameters. Batch correction among the samples was performed using Harmony [25]. Clustering was performed using addClusters with default parameters before UMAP dimensional reduction. Smoothing the dropout noise in the gene scores, included in the arrow files, was performed using addImputeWeights. Clusters were constructed by UMAP plot and the individual clusters were annotated by the pre-existing cell type-specific marker genes [10] (Table S10). High gene scores of the marker genes in the annotated clusters were confirmed by plotMarkerHeatmap. Trajectory analysis from gastric cells to IM-pit cells was performed using addTrajectory following addPeakmatrix with default parameters.

***Statistical analysis***

Unsupervised hierarchical cluster analyses were performed using R 4.0.5 with the gplots package. Volcano plot analyses were performed using R 4.0.5 with the ggplot2 package. Similarities of methylation levels of the probes were compared by Pearson's correlation coefficient. Continuous variables were compared using Welch's t test. P-values < 0.05 were considered statistically significant.



Takeuchi C, *et al. Gut* 2023;0:1–13. doi: 10.1136/gutjnl-2023-329492

# Supplementary Figure legends

***Fig. S1***

HE staining of gastric mucosa of resected specimen. Seven IM mucosa samples and eight non-IM mucosa samples were evaluated. The scale bar: 100 μm.

***Fig. S2***

Extensive DNA methylation changes in IM crypts. (a) Scatter plot analysis using methylation levels of total CpG sites. The IM and non-IM crypt samples from the same patient showed distinct DNA methylation profiles while the IM (or non-IM) crypt samples from different patients showed similar methylation profiles. Patient numbers are shown after "IM_" or "Non-IM_". (b) Unsupervised hierarchical cluster analysis using the methylation levels of the crypt samples of IM (n = 6), non-IM (n = 8), normal stomach (n = 1), and small intestine (n = 6). Left panel: Using the 20,000 CpG sites located in the CpG shore with the highest standard deviation (HSD), the IM crypt samples were separated from the non-IM crypt samples, and were clustered with the small intestinal crypt samples. Right panel: Using the 2,000 CpG sites located in intergenic CpG islands (CGIs), the IM crypt samples were clearly separated from the non-IM and small intestinal crypt samples. (c) Volcano plot analysis using DNA methylation levels of genomic blocks in promoter CGIs. The IM crypt samples showed extensive DNA hypermethylation compared with the small intestinal crypt samples.

***Fig. S3***

The clinical consequence for GC patients with IM-specific methylation profile. (a) The analysis of mucosal biopsy samples in the GEO database (accession # GSE103186). IM samples had high methylation levels of IM-specific markers. (b) Comparative analysis between the incidence of IM-type GC in the patients and the proportion of IM cells in

their total background gastric mucosa. If a patient's cancer is derived from a precursor clone with IM, it is expected to exhibit an IM-specific methylation profile. (c) Kaplan-Meier analysis of the patients with IM-type and non-IM-type GCs. The patients with IM-type GC tended to have better overall survival (OS) than those with non-IM-type GC ($P = 0.084$).

***Fig. S4***

Drug sensitivity possibly involved in IM-specific methylation profile. (a) Unsupervised cluster analysis using the IM-specific methylation markers. The gastric cancer cell lines were separated into 26 IM-type and three non-IM-type ones. (b) Sensitivity of gastric cancer cell lines to 5-FU. The two IM-type cell lines (AGS and 44As3) tended to show higher sensitivity than the two non-IM-type cell lines (GCIY and HSC60).

***Fig. S5***

Abnormal *NOS2* expression in IM cells shown by single-cell RNA-seq data [10]. (a) The t-SNE plot of cells from *H. pylori*-negative mucosa samples (n = 3) and positive mucosa samples with IM (n = 3). The cells were colored based on the samples. The clusters were clearly separated according to the *H. pylori* infection status. Potentially IM-specific clusters were shown by dotted circle. (b) The t-SNE plots with *NOS2* (right) and *CDX2* (left) expression. *NOS2*-positive cells were detected only in three *H. pylori*-positive samples.

***Fig. S6***

DNA methylation induction by *NOS2* expression in normal cells. (a) DNA methylation analysis of DOX-treated (4-week) and untreated parental cells (293FT and HGEC6B). There was no inherent effect of DOX. (b) DNA methylation analysis of DOX-treated

(10-week and 20-week) and untreated (10-week and 20-week) inducible cells (293FT and HGEC6B). *NOS2* induction was shown to induce aberrant DNA methylation ($\Delta\beta \geq 0.2$) in a large number of CpG sites. CpG sites with a β-value ≥ 0.2 are in triangles with red broken lines, and their numbers are noted. (c) DNA methylation analysis after switching DOX-off in inducible cells (293FT and HGEC6B). (d) DNA methylation analysis of NOC18-treated (10-week and 20-week) and untreated parental cells (0-week). NOC18 treatment induced slight DNA methylation. CpG sites with a β-value ≥ 0.2 are in triangles with a red broken line, and their numbers are noted.

***Fig. S7***

Enhancer and super-enhancer reprograming involved in abnormal *CDX2* and *NOS2* expression in IM. (a) Overlapping between the binding peaks of RELA and H3K27ac in the *NOS2* enhancer region. Genome browser views of ChIP-seq for RELA using a leukocyte cell line (GM12878), added to those for H3K27ac using mucosa samples. The binding peaks of RELA overlapped with those of H3K27ac. (b) Total super-enhancers identified by the ROSE program ranked by H3K27ac signal intensities. The IM mucosa gained multiple super-enhancers, including one for *CDX2*. (c) Gene ontology analysis by GREAT for the super-enhancer regions. The IM mucosa gained multiple super-enhancers related to wound healing and immune system development. The eight enriched Gene Ontology (GO) annotations are shown. Statistics: one-sided binomial test.

***Fig. S8***

Chromatin opening statuses in upstream regions of tumor-suppressor genes. The promoter regions of tumor-suppressor genes had frequent closed chromatin in IM-pit cells compared with those in all types of gastric cells.

***Fig. S9***

Trajectory analysis from gastric cells (Gastric chief_1, Gastric chief_2, Gastric pit and Gastric mucous neck) to IM_pit cells. Only an abrupt shift can be observed from gastric cells to IM-pit cells based upon the nucleosome positionings.



Takeuchi C, *et al. Gut* 2023;0:1–13. doi: 10.1136/gutjnl-2023-329492

# Reference

1 Iida N, Okuda Y, Ogasawara O, Yamashita S, Takeshima H, Ushijima T. MACON: a web tool for computing DNA methylation data obtained by the Illumina Infinium Human DNA methylation BeadArray. Epigenomics 2018;**10**:249-58.

2 Yoda Y, Takeshima H, Niwa T, Kim JG, Ando T, Kushima R*, et al.* Integrated analysis of cancer-related pathways affected by genetic and epigenetic alterations in gastric cancer. Gastric Cancer 2015;**18**:65-76.

3 Ebrahimi V, Soleimanian A, Ebrahimi T, Azargun R, Yazdani P, Eyvazi S*, et al.* Epigenetic modifications in gastric cancer: Focus on DNA methylation. Gene 2020;**742**:144577.

4 Padmanabhan N, Ushijima T, Tan P. How to stomach an epigenetic insult: the gastric cancer epigenome. Nat Rev Gastroenterol Hepatol 2017;**14**:467-78.

5 Irie T, Yamada H, Takeuchi C, Liu YY, Charvat H, Shimazu T*, et al.* The methylation level of a single cancer risk marker gene reflects methylation burden in gastric mucosa. Gastric Cancer 2023.

6 Asada K, Nakajima T, Shimazu T, Yamamichi N, Maekita T, Yokoi C*, et al.* Demonstration of the usefulness of epigenetic cancer risk prediction by a multicentre prospective cohort study. Gut 2015;**64**:388-96.

7 Maeda M, Nakajima T, Oda I, Shimazu T, Yamamichi N, Maekita T*, et al.* High impact of methylation accumulation on metachronous gastric cancer: 5-year follow-up of a multicentre prospective cohort study. Gut 2017;**66**:1721-3.

8 Kanehisa M, Goto S. KEGG: kyoto encyclopedia of genes and genomes. Nucleic acids research 2000;**28**:27-30.

9 Heinz S, Benner C, Spann N, Bertolino E, Lin YC, Laslo P*, et al.* Simple combinations of lineage-determining transcription factors prime cis-regulatory elements required for macrophage and B cell identities. Mol Cell 2010;**38**:576-89.

10 Zhang P, Yang M, Zhang Y, Xiao S, Lai X, Tan A*, et al.* Dissecting the Single-Cell Transcriptome Network Underlying Gastric Premalignant Lesions and Early Gastric Cancer. Cell Rep 2019;**27**:1934-47 e5.
11 Butler A, Hoffman P, Smibert P, Papalexi E, Satija R. Integrating single-cell transcriptomic data across different conditions, technologies, and species. Nat Biotechnol 2018;**36**:411-20.
12 Tan SH, Swathi Y, Tan S, Goh J, Seishima R, Murakami K*, et al.* AQP5 enriches for stem cells and cancer origins in the distal stomach. Nature 2020;**578**:437-43.
13 Miyoshi H, Ajima R, Luo CT, Yamaguchi TP, Stappenbeck TS. Wnt5a potentiates TGF-β signaling to promote colonic crypt regeneration after tissue injury. Science 2012;**338**:108-13.
14 Leushacke M, Tan SH, Wong A, Swathi Y, Hajamohideen A, Tan LT*, et al.* Lgr5-expressing chief cells drive epithelial regeneration and cancer in the oxyntic stomach. Nat Cell Biol 2017;**19**:774-86.
15 Yasukawa Y, Hattori N, Iida N, Takeshima H, Maeda M, Kiyono T*, et al.* SAA1 is upregulated in gastric cancer-associated fibroblasts possibly by its enhancer activation. Carcinogenesis 2021;**42**:180-9.
16 Langmead B, Salzberg SL. Fast gapped-read alignment with Bowtie 2. Nat Methods 2012;**9**:357-9.
17 Robinson JT, Thorvaldsdóttir H, Winckler W, Guttman M, Lander ES, Getz G*, et al.* Integrative genomics viewer. Nat Biotechnol 2011;**29**:24-6.
18 Whyte WA, Orlando DA, Hnisz D, Abraham BJ, Lin CY, Kagey MH*, et al.* Master transcription factors and mediator establish super-enhancers at key cell identity genes. Cell 2013;**153**:307-19.
19 Nakamura Y, Hattori N, Iida N, Yamashita S, Mori A, Kimura K*, et al.* Targeting of super-enhancers and mutant BRAF can suppress growth of BRAF-mutant colon cancer cells via repression of MAPK signaling pathway. Cancer Lett 2017;**402**:100-9.

20 Zhang Y, Liu T, Meyer CA, Eeckhoute J, Johnson DS, Bernstein BE*, et al.* Model-based analysis of ChIP-Seq (MACS). Genome Biol 2008;**9**:R137.
21 Kondili M, Fust A, Preussner J, Kuenne C, Braun T, Looso M. UROPA: a tool for Universal RObust Peak Annotation. Sci Rep 2017;**7**:2593.
22 Ramirez F, Dundar F, Diehl S, Gruning BA, Manke T. deepTools: a flexible platform for exploring deep-sequencing data. Nucleic Acids Res 2014;**42**:W187-91.
23 McLean CY, Bristor D, Hiller M, Clarke SL, Schaar BT, Lowe CB*, et al.* GREAT improves functional interpretation of cis-regulatory regions. Nat Biotechnol 2010;**28**:495-501.
24 Granja JM, Corces MR, Pierce SE, Bagdatli ST, Choudhry H, Chang HY*, et al.* ArchR is a scalable software package for integrative single-cell chromatin accessibility analysis. Nat Genet 2021;**53**:403-11.
25 Korsunsky I, Millard N, Fan J, Slowikowski K, Zhang F, Wei K*, et al.* Fast, sensitive and accurate integration of single-cell data with Harmony. Nat Methods 2019;**16**:1289-96.